# Study of the effects of shading in thin-film perovskite PV modules

Sujith Vishwanathreddy


Delft University of Technology

TU Delft

# Study of the effects of shading in thin-film perovskite PV modules

by

Sujith Vishwanathreddy

in partial fulfilment of the requirements for the degree of Master of Science in Sustainable Energy Technology
at the Delft University of Technology, to be defended publicly on Thursday, 25th of August, 2022 at 14:00.

| | | | |
|---|---|---|---|
| Student number: | 5217504 | | |
| Project duration: | Nov 2021 - Aug 2022 | | |
| Thesis committee: | dr. I. Gordon | TU Delft/Imec | Supervisor |
| | dr. A. Aguirre | Imec | Daily supervisor |
| | dr. P. Manganiello | TU Delft | Internal committee member |
| | dr. Z. Qin | TU Delft | External committee member |
| Additional supervision: | ir. J.Sala | Imec/UHasselt | Daily supervisor |

An electronic version of this thesis is available at http://repository.tudelft.nl/.

TU Delft

# Preface

The thesis project is the culmination of my Master's degree in Sustainable Energy technology at TU Delft. It was an incredible opportunity to apply the knowledge from the courses and gain valuable practical experience at the lab in Energyville. With the project, I was introduced to perovskites which is an exciting upcoming PV technology, by investigating its response to partial shading.

The project would not be possible without the guidance and support of many people. First of all, my supervisor from TU Delft and Imec, dr. Ivan Gordan. Thank you for your feedback during the meetings, and encouragement after each presentation; it boosted my confidence and pushed me to think critically. Further, I would like to thank my daily supervisor, dr. Aranzazu Aguirre (Arantxa) for making the time to help me with any clarifications regarding the project and regular discussions at the lab. Your jovial nature made it easy for me to approach even for small queries. Furthermore, thankful to Jacopo for the insights during the discussions which helped me strengthen my fundamentals on the subject.

Special thanks to the entire Thin Film PV group at Energyville. I felt welcome since the first day and learned so much through my interactions with each one of them. Appreciate the time taken by the Ph.D. students, especially Santosh and Sownder for discussing openly about the project and sharing their insights. Thankful to Anurag for the insightful conversations about the degradation of perovskites. Many thanks to Tom Aernouts for making the stay hassle-free and the support. Lastly, thanks to Pavithran, my fellow thesis student for making the entire project enjoyable and fun.

During the Master's program, I had the pleasure of meeting some interesting people who added much value to my journey. Thankful to all my classmates, JIP team, and team members from the group projects I was a part of. Finally, the team at Biosphere Solar, working with them was a great boost to my holistic learning experience and hugely grateful to be a part of the team. Especially Si, Perine, and Maitheli, I learned so much from all of them and grew so much personally.

Finally and most importantly, I am grateful to my family for supporting me financially, emotionally, and in every way possible. Without them, this would have still been a dream.

*Sujith Vishwanathreddy*
*Hasselt, August 2022*

# Abstract

People worldwide have begun to feel the effects of climate change in recent years with unpredictable weather patterns, heatwaves, changes in precipitation, and sea level rise. To help mitigate climate change, photovoltaics (PV) is seen as a technology with the tremendous capability to satisfy the world's electricity demands by tapping into renewable energy from the sun. There are various PV technologies available, each with its challenges; the newest upcoming material is perovskites. They have showcased an immense potential of further lowering the production costs of solar modules, lower material consumption, and promising high conversion efficiencies. The single cell efficiency has seen incredible improvement in the last decade to 25.7%. The next stage is the scaling up to module level and outdoor deployment. However, some significant challenges remain towards achieving this; one is its response to shading, which has been studied little thus far and will be investigated in this study.

The increasing integration of PV into the close surroundings also means that integrated PV will be exposed to much more shading than a typical panel in a solar farm. It is imperative to understand the behavior of perovskite solar cells (PSCs) to shade, primarily due to the poor reverse bias behavior reported in recent years. Since the cells are typically connected in series, shaded cells dissipate energy by going into negative voltages. The response to shading of any material also depends on the interconnection method adopted for the solar cells. So, several interconnections were identified in the project, a few including bypass diodes to improve shade tolerance. Due to the poor reverse bias characteristics of the PSCs, the interconnections and shading were modeled using Matlab and Simulink to better understand the interconnection configuration with the least power mismatch losses. Total Cross Tied (TCT) with bypass diodes was identified as the optimal configuration.

Furthermore, the TCT interconnection with bypass diodes was tested experimentally on a shading setup to validate the model. The experiments confirmed the modeled results. None of the modules degraded under shading for the interconnection as the cells did not experience large enough reverse bias voltages. Additionally, tests were conducted to gain deeper insights into the degradation mechanism of perovskites. Shading was tested on a single module, parallel and perpendicular to laser scribes, to confirm that the degradation was due to reverse bias voltage. When the module was exposed to an Electroluminescence (EL) test after shading, it revealed the degradation through the formation of dark spots. The degradation is speculated to form due to the formation of shunt paths caused by the migration of copper into the absorber layer. A similar test was conducted on semi-transparent modules that did not lead to degradation. Also, the modules were tested to find their reverse breakdown voltage. It was observed to breakdown at -6.5V, translating to a cell breakdown at -1.6V. Interestingly, the module's performance was slightly regained under light soaking for one hour in forward bias due to the reversal of the ion movement, which occurred in the reverse bias condition. The research into the shading of PSCs is still in the early days; many further topics for the future are proposed that could be interesting for later research.

# Contents

# List of Figures

# List of Tables

# Acronyms

## Abbreviations

| Abbreviation | Definition |
|---|---|
| GHG | Green House Gas |
| TPES | Total Primary Energy Supply |
| PV | Photovoltaic |
| I | Current |
| V | Voltage |
| $I_{sc}$ | Short circuit current |
| $V_{oc}$ | Open circuit voltage |
| MPP | Maximum Power Point |
| $V_{mpp}$ | Voltage at Maximum Power Point |
| $I_{mpp}$ | Current at Maximum Power Point |
| FF | Fill Factor |
| PCE | Power Conversion Efficiency |
| HTM / HTL | Hole Transport Material / Hole Transport Layer |
| ETM / ETL | Electron Transport Material /Electron Transport Layer |
| $V_{bd}$ | Reverse breakdown voltage |
| $V_d$ | Forward voltage of diode |
| PSC | Perovskite Solar Cell |
| S-P | Series-Parallel |
| TCT | Total Cross Tied |
| SP | Shading Pattern |
| ITO | Indium Tin Oxide |
| Cu | Copper |

# 1

# Introduction

Section 1.1 will discuss the contribution of energy generation to the effects of climate change and the need for a transition to cleaner sources. Technology development often takes many decades to develop; section 1.2 examines the development of the solar cell as we see it today, tracing back to the discovery of the photoelectric effect in 1839. The division of the different PV technology categories will be briefly reviewed in section 1.3. section 1.4 lays out the research objectives for the thesis. Lastly, the outline for the report is briefly discussed in section 1.5

## 1.1. Climate change and energy transition

Economic development for raising people's living standards across the globe and achieving many of the sustainability goals set out by the United Nations (UN) is closely linked with energy consumption [1]. Unfortunately, the global total primary energy supply (TPES) since the advent of the industrial revolution that started over 200 years ago has been primarily dominated by fossil fuels. Burning fossil fuels to meet the TPES leads to increased concentrations of GHGs in the atmosphere responsible for climate change. As seen in Figure 1.1, over 80% of the GHG emissions have been for energy generation in different forms in 2008. The TPES includes all activities that require energy like the production of goods, transformation, transportation, heating, and electricity generation.

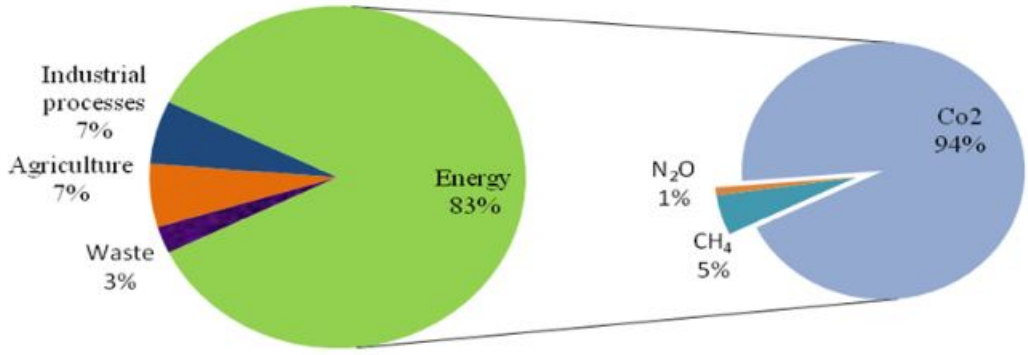


**Figure 1.1:** Share of anthropogenic GHG emissions in Annex 1 countries in 2008 [1]

In 2015, a collective of 195 countries signed the Paris Agreement to limit temperature rise below 2°C, making governments worldwide take notice of the problem [2]. The global GHG emissions increased in the last decade, but the rate of increase has reduced to 1% per year between 2011 and 2019 compared to 3% in the previous

decade [3]. The agreements between countries have slowed down the growth of emissions in some industrialized countries, but further cooperation and advancements toward non-polluting technologies are necessary for a rapid turnaround.

Consequently, there is a need for alternate ways of producing energy that is more sustainable. In this regard, energy from the sun that is renewable and cleaner is one with immense potential. Especially with the recent advancements, which include an exponential drop in prices and higher efficiency of the solar cells per unit area, one of the most promising technologies for the energy transition is photovoltaics (PV). Currently, solar energy meets 3.2% of the global electricity demand compared to an almost null contribution only a few decades ago. The cost of electricity generation from solar has dropped between 3 to 6 euro cents per kWh depending on the region [4]. In many places, the price of electricity is even lower than conventional energy sources, making it possible to compete in the energy market without any subsidies from the government. As a result, the number of solar panel installations has been growing at an increasing rate worldwide since 2010, as shown in Figure 1.2.

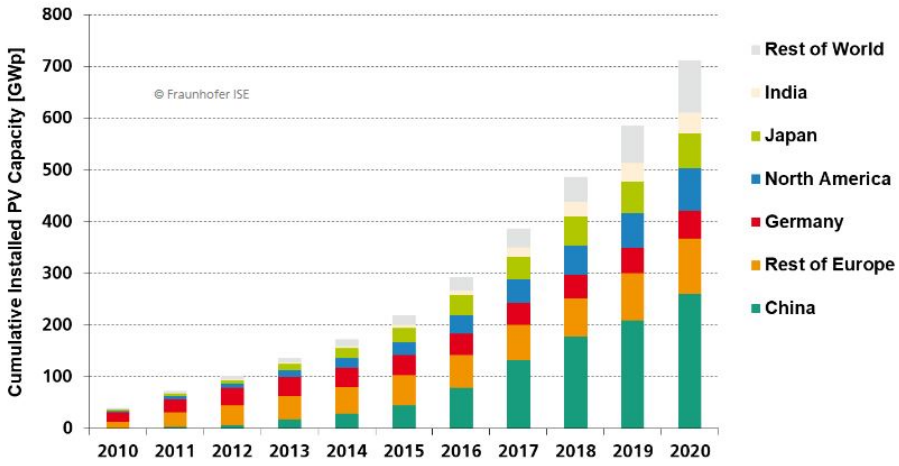


**Figure 1.2:** Growth in solar PV in the last decade [4]

## 1.2. Brief history of solar cell technology

Developing any technology often takes many decades with the involvement of many stakeholders, and it is no different for PV. In 1839, the photovoltaic effect, i.e., generation of electric current in a material when exposed to light, was first observed by a French physicist, Alexandre Edmond Becquerel, when he was conducting electrochemical experiments involving the exposure of silver and platinum electrodes to sunlight. The effect was first published in the scientific community several decades later in 1873 when Willoughby Smith wrote in that year's Nature journal describing the effect of Selenium on light exposure. Furthermore, six years later, the first solar cell was developed by Charles Fritts by coating Selenium with a layer of gold to form the two polar junctions. Despite the device was only 1% efficient, it was demonstrated for the first time that solar energy could be transformed into electricity through solid material without the involvement of any moving parts [5] [6].

However, the observed effect was little understood, and a theory explaining the underlying principle was necessary. It was not until 1905 that Albert Einstein proposed the photoelectric theory to explain the physics and develop mathematical formulations. The theory considered light to have a dual nature of wave and particle. The particle nature extends to explain that photons are made up of packets of energy called "quanta", with energies corresponding to different radiation frequencies. A threshold frequency is necessary to liberate electrons in given material resulting in the current flow. It is the fundamental principle used to explain the working of a solar cell even today [7] [8].

The possibility of developing technology that takes advantage of the photoelectric effect took many decades. In 1925, Bell Telephone Laboratories was founded in the United States of America primarily to research and engineer solutions for the telecommunications industry. Bell Labs was one of the pioneers in developing microelectronics using semiconductors [9]. In 1939, Russel Ohl at Bell Labs discovered the photoelectric effect in silicon. He developed the n- and p-type regions by adding impurities responsible for creating the electric field to facilitate the movement of electric charges. In the subsequent year, Ohl developed the first silicon solar cell, which at the time was utilized as light sensors due to its extremely low efficiency. Calvin Fuller, a chemist at Bell Labs several years later in 1954, developed a process to dope silicon, which resulted in an efficiency of 6% in converting the solar energy into electrical energy by doping boron and arsenic, which was an incredible achievement at the time [10] [6].

The interest in photovoltaics expanded in the following decades with the growing interest in space exploration through NASA and other space programs worldwide. It was one of the main drivers for innovation in the early stages of the technology, leading to investments in research and development mainly to support the satellite communication systems as depicted in Figure 1.3. The technology at the time was not within reach of the public due to the challenges in scaling up the manufacturing to drive down the costs. However, it helped showcase the enormous potential of harnessing renewable energy from the sun. [10].

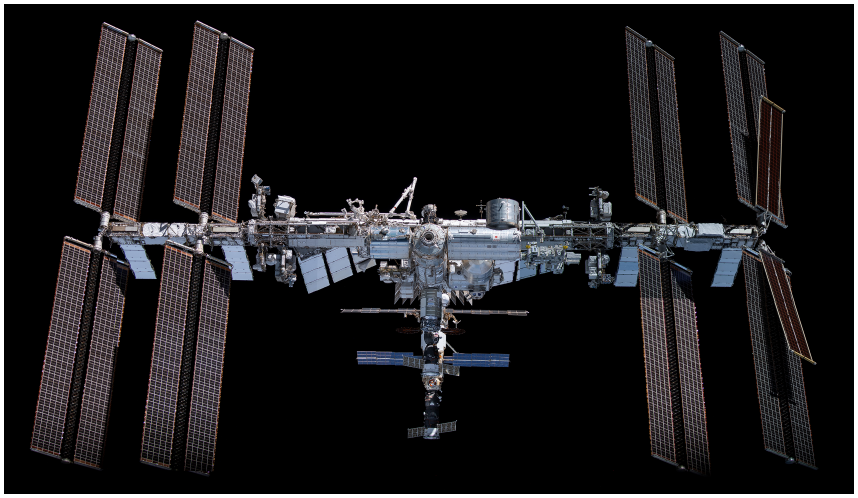

**Figure 1.3:** Solar panels installed at the International Space Station (ISS) [11]

Until the end of the 20th century, solar cells were manufactured mostly using silicon as the photo-active material. Until 2010, the market was mainly dominated by multi-silicon with a lesser proportion from mono-silicon, and marginal contribution from thin-film technologies. As of 2020, mono-silicon is quickly replacing multi-silicon due to negligible cost difference in manufacturing mono-wafers. The thin film technologies that occupy a smaller market share are currently dominated by Cadmium Telluride (CdTe), with about 4% of the total market share [4]. Some concerns are raised about silicon regarding its high material consumption and saturation in the highest efficiencies possible with the material. The race to further lower the costs of technology and resource consumption has led to newer technologies which will be explored in the next section [10].

## 1.3. Photovoltaic technologies

Many photovoltaic technologies have been invented in recent decades, and some have also scaled up for commercialization. These can be broadly divided into three generations, as shown in Figure 1.4. The main criterion for the distinction comes from the materials and fabrication techniques used for the production.

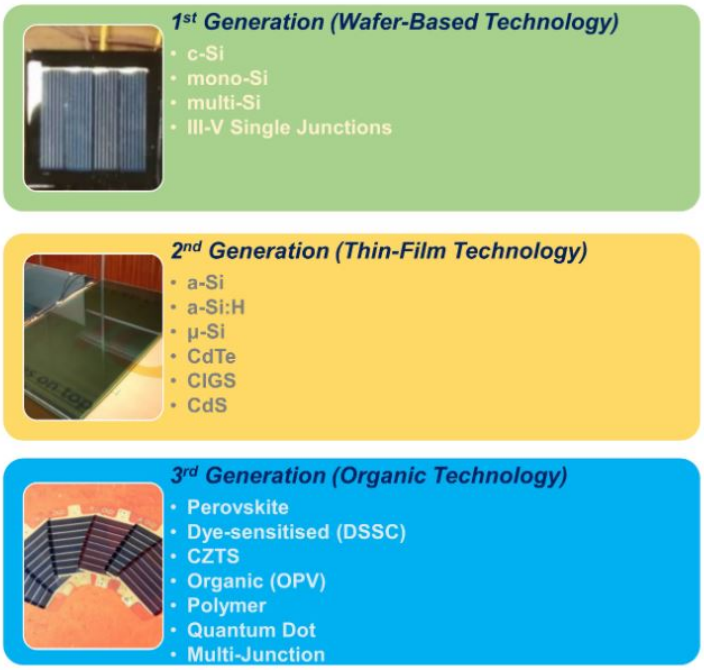


**Figure 1.4:** Different generations of PV technologies [10]

The first generation of PV mainly dominates the market and, as of 2020, accounts for 95% of the market share [4]. The industry relies heavily on silicon for its manufacturing as it benefited from the already established manufacturing process for high purity silicon from the semiconductor industry for producing microchips [6]. Another factor in the popularity of silicon is its bandgap. It determines the spectrum of the light emission from the sun that can be absorbed by the solar cell. With a bandgap of 1.12 eV, it is within the range for the high efficiencies possible according to the Shockley Quisser limit, as seen in Figure 1.5. However, silicon has an indirect bandgap resulting in a low absorption coefficient, leading to the need for thicker absorber layers because a photon and phonon (lattice vibration) is required to create electron-hole pair. Since its first discovery of photovoltaic properties, the efficiency has increased significantly from 6% to a record efficiency of 26.7% at the lab [12]. Some notable breakthrough in the processing at the industrial in wafer processing and multi-wire sawing has helped reduce the costs of the cell available in the market. Apart from silicon, other materials are used, belonging to the III-V category like Gallium Arsenide (GaAs) and Indium Phosphide (InP), to name a few. These materials possess a direct bandgap and have higher efficiencies, but due to their high material costs are used primarily in space applications, and solar concentrators [10].

One of the major concerns of the wafer-based technology was its high material consumption. The second generation of PV cells, called thin film technology, tries to counter this problem with a significantly narrower absorber layer in the range of a few micrometers as compared to a few hundreds of micrometers as seen in the earlier generation. Initially, the efficiency achieved was lower due to the smaller absorption layer. However, the efficiencies were improved with new fabrication techniques like spray coating and other vacuum-based methods. The efficiency can now compete with the existing market leaders with a current highest record of 23.4% using CIGS as the absorber layer. The fabrication flexibility allows for its usage in many other areas unimaginable with earlier generations, like flexible substrates for wearable gadgets and many more. Another significant advantage is that the temperature required in the processing is significantly lower, resulting in lower GHG emissions and energy payback time [10].

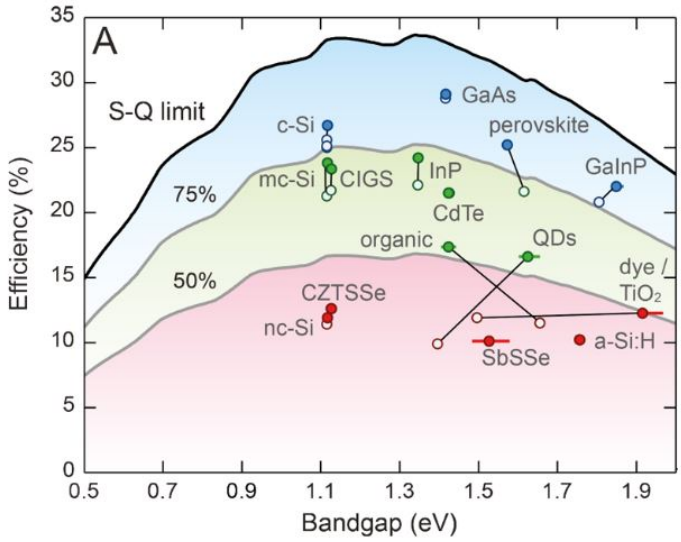


**Figure 1.5:** Comparison of different PV technology efficiencies to the Shockley-Quisser limit (Open symbol shows record efficiency in 2016 and the solid symbol represents in 2020) [13]

The third generation of cell technology stems from thin film technology, which can be made with different materials like organic compounds. Newer cell architectures different from the p-n junction make it possible for better efficiencies. One of the critical advantages of this technology is the ability to tune the bandgap to capture different parts of the solar spectrum. This property is beneficial in creating multi-junction solar cells, which make it possible to achieve even higher efficiencies by stacking two or even three photovoltaic materials on each other in series connection to capture a larger part of the solar spectrum. One of the materials garnering much attention in the last decade is perovskites, with cell efficiencies reaching 25.7% from just 3.8% in 2009. The rise in conversion efficiency is unseen with the other materials, and its low cost in manufacturing, among other benefits, makes it a strong contender to substitute the incumbents.

However, many questions remain regarding the scaling up of perovskites. One among them is its response to shading, which has been studied little thus far. It is a critical criterion to be satisfied for the outdoor deployment of any PV technology. As a consequence, the focus of this study will be to develop and understand the effects of partial shading on the material and possible strategies to minimize the effects with alternate interconnection configurations. It is further elaborated in chapter 2.

## 1.4. Thesis research objectives

The main objective of the thesis is to understand the behavior of perovskite solar cells to shading and explore alternate interconnection topologies to minimize its effects. The initial literature study for the topic involved understanding the combinations of cell interconnections tested by other researchers to improve the performance

under different shading scenarios. Due to its popularity in the market, the research papers were dominated mainly by silicon cells. Nevertheless, it provided a foundation for understanding the behavior of different interconnections and selecting the interesting ones for this study. However, it was clear that the behavior of perovskite solar cells would differ significantly due to the difference in their current-voltage characteristics.

The following research question was formulated for the study:

**Can the performance and degradation of perovskite solar cells be improved under different shading conditions by using alternate interconnections?**

The research question is divided into sub-questions to guide the study and aid in answering the main question. These are as follows:

- How can the interconnections be modeled for a deeper understanding to guide the experiments?
- Which interconnection configuration results in minimum overall power mismatch losses for different shading conditions, and can it be tested experimentally?
- What are some potential mechanisms for the degradation, and can other tests provide insight into the behavior?

For the modeling, Matlab and Simulink will be utilized. The reason for choosing Simulink is due to the already available tools for electrical simulations and prior experience with the software by the author. The modeled results will be tested experimentally to check for conformance. The above sub-questions will be addressed more in detail in the upcoming chapters.

## 1.5. Outline

The posed research questions are answered in the upcoming chapters. Chapter 2 provides the essential theoretical understanding necessary for the thesis. The initial sections cover the fundamentals of a solar cell's working. Perovskite materials are introduced in section 2.6, followed by mechanisms describing the reverse breakdown behavior of PSCs in section 2.4.

In chapter 3, the experimental details are elaborated. The perovskite minimodules used for conducting the experiments are mentioned in section 3.1. The shading setup used for conducting the experiments is briefly addressed in section 3.2. The four different interconnections that were modeled are discussed in subsection 3.2.1 to subsection 3.2.4. The effect of bypass diodes on cell interconnections is elaborated in section 3.3.

The research methodology is introduced in chapter 4. The different steps are briefly discussed in section 4.1. Shading patterns and the interconnection configurations on which they are tested is presented in section 4.2 and section 4.3. The Simulink model for simulating the interconnections and shading is introduced in section 4.4.

The results from the study are showcased in chapter 5. In section 5.1, shading tests performed on a single module are discussed. The simulation results are presented in section 5.2. Experiments performed on the setup are discussed in section 5.3. Finally, the simulation and experiments results are compared in section 5.4.

Additionally, experimental tests were conducted to gain deeper insights into the degradation mechanism, illustrated in chapter 6. The results from the electroluminescence test is discussed in section 6.1. Tests to find the reverse breakdown and recovery under light soaking are mentioned in section 6.2 and section 6.3 respectively. Semi-transparent modules were tested for their response to shading and presented in section 6.4.

Finally, chapter 7 concludes the report. The outcomes of the thesis are briefly outlined in section 7.1 along with some recommendations and future research areas to understand better shading response of perovskites.

# 2

# Theory

In the following sections, some essential theoretical concepts are introduced. Section 2.1 provides a basic understanding of the working of a solar cell. An equivalent circuit represents a solar cell, described in section 2.2. The current-voltage curves and their effect on changes in illumination are elucidated in section 2.3. In section 2.4, the working of a solar cell in positive and reverse voltages is explained. The effect of partial shading on solar cells is demonstrated in section 2.5. Finally, section 2.6 provides an overview of the origin of perovskites and some challenges in commercializing the technology.

## 2.1. Solar cell working principle

The solar cell works on the principle of the photoelectric effect. To create a solar cell, two oppositely doped (addition of impurities) materials are combined as depicted in Figure 2.1. In the space between the two doped regions lies the depletion region (shaded in the figure), which is devoid of charges due to the movement of ions from either side. When this cell is exposed to illumination, electron-hole pairs are created. The two opposite polarities on either side produce an electric field that helps separate the charges generated due to radiation. The electrons move towards the negative polarity (n-side), and the holes drift towards the positive side (p-side).

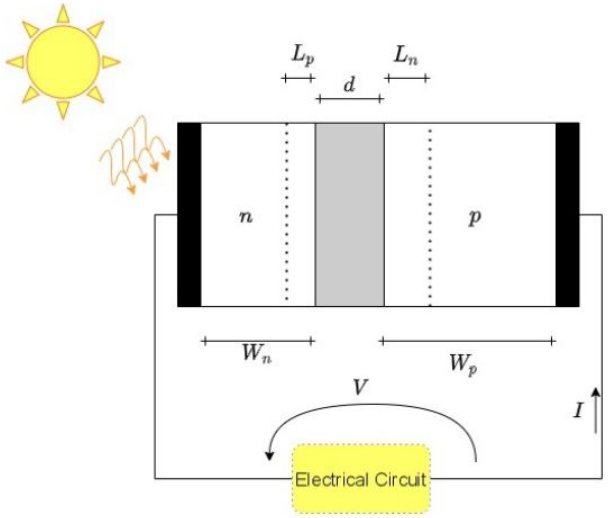


**Figure 2.1:** Working of a solar cell [10]

Now, an external circuit can be connected across the two polarities. The charges are accumulated on either side and flow through the circuit, leading to a current that can perform practical work. Many such cells are interconnected to make a whole module installed on rooftops or other locations to harness the energy from the sun.

## 2.2. Equivalent solar cell circuit

The above-described solar cell is simplified to an equivalent circuit to perform mathematical calculations and aid in modeling. For this project, a single diode model was used to perform the simulation, as shown in Figure 2.2.

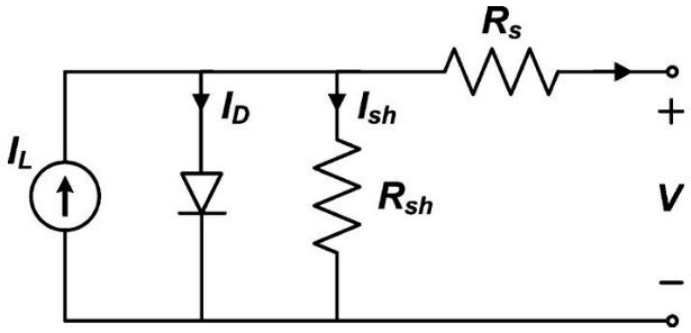


**Figure 2.2:** Single diode equivalent solar cell circuit [14]

The equivalent circuit consists of a current source, diode and resistances .$R_{sh}$ represents the shunt resistance, i.e., alternative paths for the current flow between the front and back surfaces due to mechanical defects and dislocations in the material [14]. It is preferable to have a high resistance value as it signifies fewer current paths and defects in the cell. Series resistance denoted by $R_s$ signifies the resistance offered to the current flow between the semiconductor layer and the two contacts connecting to the external circuit. The series resistance should ideally be as low as possible as it means an easier flow of the charge carriers. The current generated due to the illumination in the cell is called photocurrent and is represented as $I_L$. Lastly, the current through the diode is shown as $I_D$. [15]

The current in the external load, I, is given by the following equation using Kirchoff's current law,

$$I = I_L - I_D - I_{sh} \tag{2.1}$$

After substituting the Shockley diode equation and applying Ohm's law, the equation for the solar cell current is represented as:

$$I = I_L - I_o(e^{\frac{qV}{nkT}} - 1) - \frac{V - IR_s}{R_{sh}} \tag{2.2}$$

$I_o$ is the reverse saturation current representing the diffusion and recombination of electrons and holes. The ideality factor, n, is equal to 1 if the dark current, i.e., current under no illumination, is solely determined by the diffusion of charge carriers. The ideality factor is greater than one if the recombination in the depletion region also contributes to the diode current ($I_D$). The constant k is Boltzmann's constant equal to $1.38 * 10^{-23} m^2 kg s^{-2} K^{-1}$ and q is the charge of an electron with a value of $1.6 * 10^{-19} C$. Lastly, T represents the temperature of the cell [15].

## 2.3. Current-voltage (I-V) curve

Equation 2.2 when plotted on a graph is represented in Figure 2.3. The current at the short circuit condition, i.e., zero voltage, is termed short circuit current ($I_{sc}$). Similarly, the voltage at open-circuit condition, i.e., zero current, is termed open-circuit voltage ($V_{oc}$). The power generated from the solar cell is determined by multiplying the current and corresponding voltage. As seen in the figure, the power reaches a maximum point at a particular voltage level ($V_{mpp}$), and this point is termed the maximum power point (MPP). The corresponding current at the voltage is denoted by $I_{mpp}$. The slope of the curve at the short circuit and open circuit conditions represents the shunt and series resistance, respectively.

The maximum power retrieved from a solar cell is represented by the area shaded in blue in the figure. The power is generated only when both current and voltage are positive. However, when either is negative, the solar cell dissipates energy in the form of light and heat energy. It is an essential factor when discussing shading and will be explained further in the upcoming chapters.

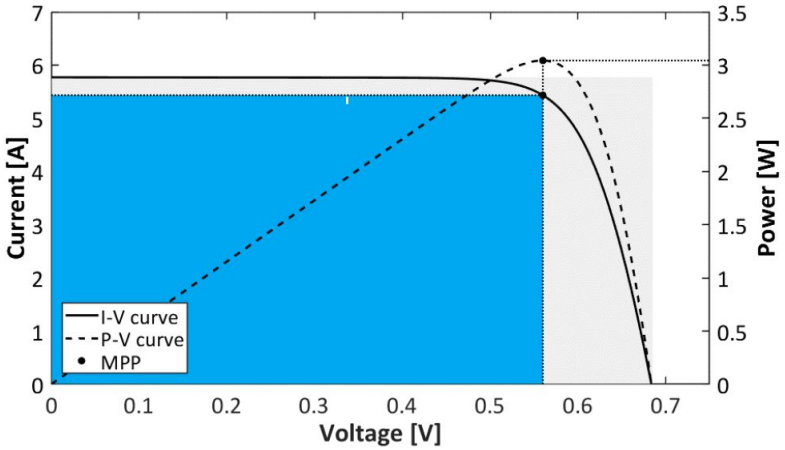


**Figure 2.3:** I-V and P-V curve for a typical silicon solar cell [16]

Another important parameter when discussing the solar cell characteristics is the fill factor (FF). It is desirable to have a fill factor that is as high as possible. It is defined as follows:

$$FF = \frac{Area_{blue}}{Area_{grey}} = \frac{I_{mpp} * V_{mpp}}{I_{sc} * V_{oc}} \tag{2.3}$$

The current generated in the solar cell is proportional to the irradiance on the solar cell, as seen in Figure 2.4. In other words, a cell with lower irradiance will produce a lower amount of current [17]. In a solar module with many interconnected cells, partial shading can generate different current levels in various cells. It can have some severe effects on the solar cells, which will be emphasized in section 2.5

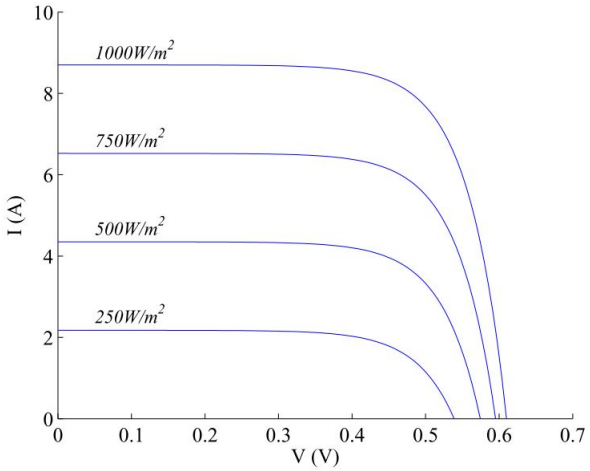


**Figure 2.4:** Current-voltage (IV) parameters under different illumination level of a simulated silicon solar cell [18]

## 2.4. Reverse breakdown voltage

A solar cell, when not illuminated, will have similar I-V characteristics as that of a diode. The operating range of a diode can be divided into three regions as depicted in Figure 2.5. The solar cell in working condition is designed to operate in the forward bias region of the curve. When under illumination, the curve would be shifted downwards due to charge carriers generated due to illumination as shown in Figure 2.3 (the graph is inverted). However, the solar cell can experience negative voltages under certain operating conditions and operate in the reverse region. If the voltage is increased in the reverse direction beyond a certain magnitude, depicted in the figure as $V_{br}$, the cell would reach its breakdown limit and degrade as a consequence. Often this degradation is irreversible, hence making the damage permanent.

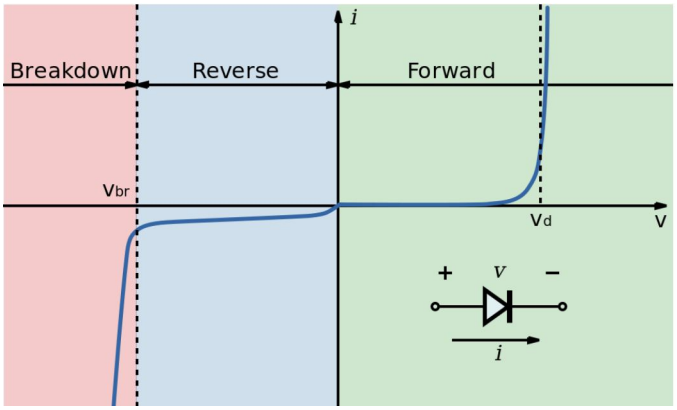


**Figure 2.5:** Diode current-voltage characteristics [19]

Typically in a solar panel, many solar cells are stringed together in series. The reverse bias voltages are experienced in the cells when cells in the string experience a lower illumination than the other cells. In Figure 2.7, it illustrates series interconnection of six solar cells each with $V_{oc}$ of about 0.5V. However, one of the cells is shaded partially, leading to lower photocurrent and hence a decrease in $I_{sc}$. Since the cells are connected in series, the current in the string is equal to the current generated in the worst performing cell (shaded one). Part of the energy generated in the unshaded cells will be dissipated on the shaded cell as represented in Figure 2.6. This energy dissipation can have detrimental effects on the cell's life and will be explored in the next section.

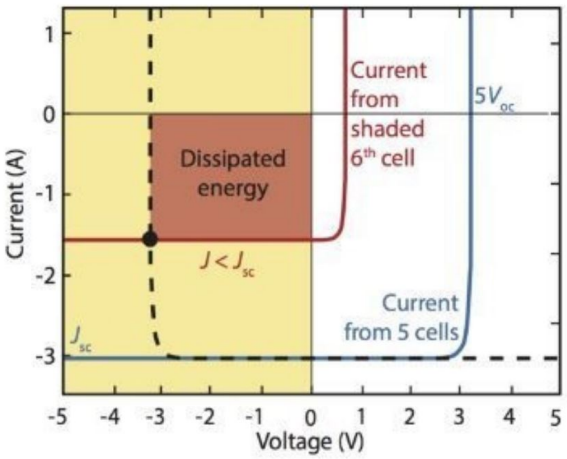


**Figure 2.6:** Reverse bias voltage development in series connected cells [17]

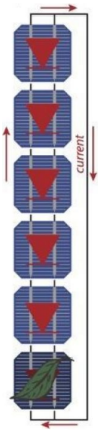


**Figure 2.7:** Shading of a cell in a string of series interconnection [17]

## 2.5. Effect of partial shading

When installed in the outdoor environment, a typical solar panel experiences different conditions compared to the lab's controlled conditions. One of the differences is the presence of shadows on the panel due to nearby buildings, the passing of clouds or trees in the close vicinity. It leads to non-uniformity in the illumination of the different cells in the solar panel. The difference in the illumination leads to a reduction in the device's power output. Often, a drop in performance can be case-specific as it varies depending on the solar cell technology. Currently, the PV technology that is widely used is Silicon, and the cells are connected in a series configuration to increase the output voltage and reduce the resistive losses in the solar module. However, the series interconnection leads to the building up of high reverse bias voltage across the shaded cells leading to dissipation of energy in the form of heat. It can lead to degradation of the corresponding cells by the formation of hotspots, as shown in Figure 2.8. Hotspots are formed due to the cell's current flow through small shunt paths. The passage of high current leads to heat generation, several degrees higher than unshaded cells [20].

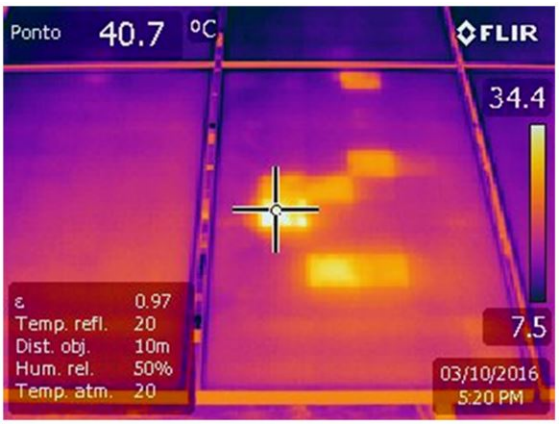


**Figure 2.8:** Thermal picture showing the increase in temperature of shaded cells [20]

The shading experienced by the solar panel can be of two types: complete and partial shading. Complete shading refers to a decreased illumination of all the cells in the panel, for example, during night time. In contrast, partial shading refers to a variation in the illumination of the different cells. The partial shading condition is the case that significantly affects the performance and the lifetime of the cells. With the ever-increasing integration of PV into our immediate environment, like building integrated PV (BIPV) and vehicle integrated PV (VIPV), shading will be a significant concern in deploying PV technology.

## 2.6. Perovskites

The perovskite structure (as shown in Figure 2.9) was first discovered in nature as an oxide with a chemical formula of $CaTiO_3$. Gustav Rose found it in the Ural mountains in Russia in 1839. The name 'perovskite' originates from the last name of a famous Russian mineralogist by the name of Count Lev Aleksevich von Perovski (1792-1856) [21]. Perovskite is now referred to chemical compounds with the same crystal structure as that of $CaTiO_3$ [22]. Perovskite solar cells consist of organic molecules, metal elements, and halides. They have a chemical formula represented as $ABX_3$. 'A' is a monovalent cation that typically consists of organic compounds like Methylammonium (MA) $(CH_3NH_3^+)$ or Formamidinium (FA) $(HC(NH_2)_2^+)$, and also inorganic elements like Cesium (Cs). 'B' can be associated with a divalent cation. Usually, lead (Pb) and some recent research include Tin (Sn). 'A' is usually of larger molecular size compared to that of 'B' ion. Lastly, 'X' is an anion consisting of halides like Bromine (Br), Chlorine (Cl), or Iodine (I). Usually, the perovskite composition can contain varying proportions of the ions mentioned, such as 80% MA and 20% Cs, to make up the structure for additional benefits like bandgap tuning [23] [24] [25].

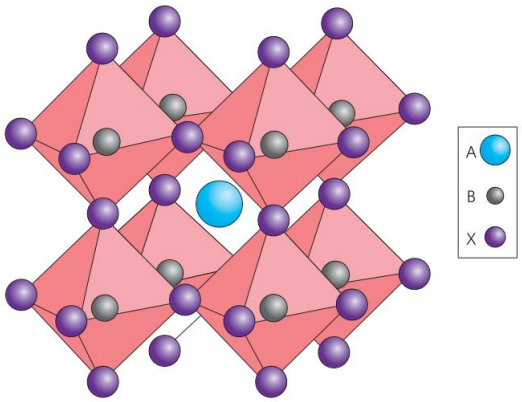


**Figure 2.9:** Perovskite crystal structure [23]

The first characterization studies showing the photoconductive properties of $CsPbX_3$ were carried out in the 1950s by a Danish scientist, Christian Moller. In 1978, Caesium was replaced with methylammonium (MA) cations to generate the first combination of organic and inorganic hybrid perovskites. The optical and electronic properties of methylammonium iodide $(CH_3NH_3PbI_3)$ have been carefully studied in the last few decades. It has a direct bandgap of 1.55 eV, and the absorption of the spectrum is until 800 nanometers (nm) of wavelength in the solar spectrum. The charge carriers created by light absorption have weak binding energy of 0.03 eV, dissociating quickly even at room temperature. The generated electrons and holes possess high carrier mobilities and longer carrier diffusion lengths, resulting in reduced recombination of charge carriers within the absorber layer [26].

One of the main reasons for the widespread attention towards perovskites is the rate at which light absorption efficiency was improved in a short time interval that is unparalleled with the other materials in the past. In 2009, when $(CH_3NH_3PbI_3)$ and $(CH_3NH_3PbBr_3)$ (larger band gap) were introduced as sensitizers for liquid electrolyte based Dye Sensitised Solar Cells (DSSC). It resulted in only 3.8% of power conversion efficiency (PCE), and the perovskite dissolved in the organic solvent. Within just three years, the researchers achieved a PCE of 6.5% by changing the electrolyte formulation and deposition method [26] [27].

However, as the interest in these materials grew worldwide, researchers began to notice some concerns. Perovskites tend to degrade in high humidity conditions and temperatures, so extensive tests are necessary to prove their viability in the outside environment. There are concerns with the usage of lead as it is widely known to be carcinogenic; however, its usage per weight is still relatively small. Nevertheless, alternative materials need to be investigated, like Tin. Due to its instability and tendency to form intermediate phases when a voltage is applied, hysteresis is observed in the performance measurements (I-V scans), which leads to non-repeatability of the tests [26]. Finally, it was recently discovered that perovskites tend to degrade when there is a reverse bias voltage applied across the cell terminals and have a low reverse bias breakdown voltage in the range of just 1 and

4 volts, as shown in Figure 2.10 [28]. According to recent studies in the area, it is suspected that the reason is due to the creation of mobile ions. It is a big concern when discussing its performance in the outside environment because series connected cells lead to reverse bias voltage development when shaded. The report in the upcoming chapters will address this issue in more detail and possible use of alternate interconnections to reduce the effect.

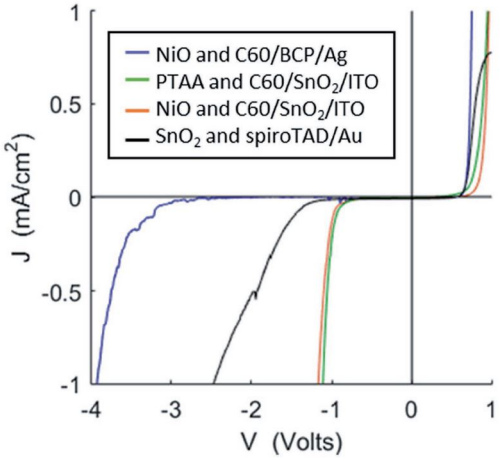


**Figure 2.10:** J-V measurement showing reverse breakdown for $Cs_{0.17}FA_{0.83}Pb(I_{0.83}Br_{0.17})_3$ with different charge transport layers [28].

## 2.7. Reverse bias degradation mechanism

The poor reverse bias behavior of PSCs has garnered attention from researchers in the last two to three years and is cited as one of the major challenges in scaling up the technology. Some theories have been developed that back the experimental observations to gain a deeper understanding to reduce its effects; the drift-diffusion model is the popular one that can explain most of the effects. One of the main reasons for the effect is the existence of mobile ions that lead to the bending of the band diagram as depicted in Figure 2.11. Most studies present iodine vacancies as the main mobile species initiating the degradation [29] [30].

According to the drift-diffusion model, the reverse current observed under negative voltage occurs due to the tunneling of the charge carriers from the transport layers into the perovskite absorber layer due to the high electric field at the interface. This is in contrast to the avalanche breakdown observed in silicon solar cells, which require higher voltages to cause impact ionization [31]. As seen in Figure 6.7a, an electric field is created due to the two doped transport layers to facilitate charge collection. Due to the built-in field, positive vacancies drift towards the HTM and are collected at the absorber/HTM interface. At the interface with the ETM, a depletion region similar to a Schottky barrier is formed as shown in the figure [28].

Later, a reverse bias voltage of 1V is applied across the contacts, as seen in Figure 6.7b. It leads to further bending of the band diagram near the ETM interface, as depicted in Figure 6.7b. However, the voltage of -1V is not sufficient to allow for the tunneling of holes into the absorber layer. However, as the reverse voltage is increased in Figure 6.7b, the band bending is more significant, and holes can tunnel from the ETM layer to produce current. Due to asymmetrical bending of the band diagram, it results in the injection of one type of charge carrier at reverse bias voltages. The holes that are injected into the absorber layer lead to the oxidation of iodine ions, contributing to the formation of neutral iodine interstitials and iodine vacancies [28] [32] [33].

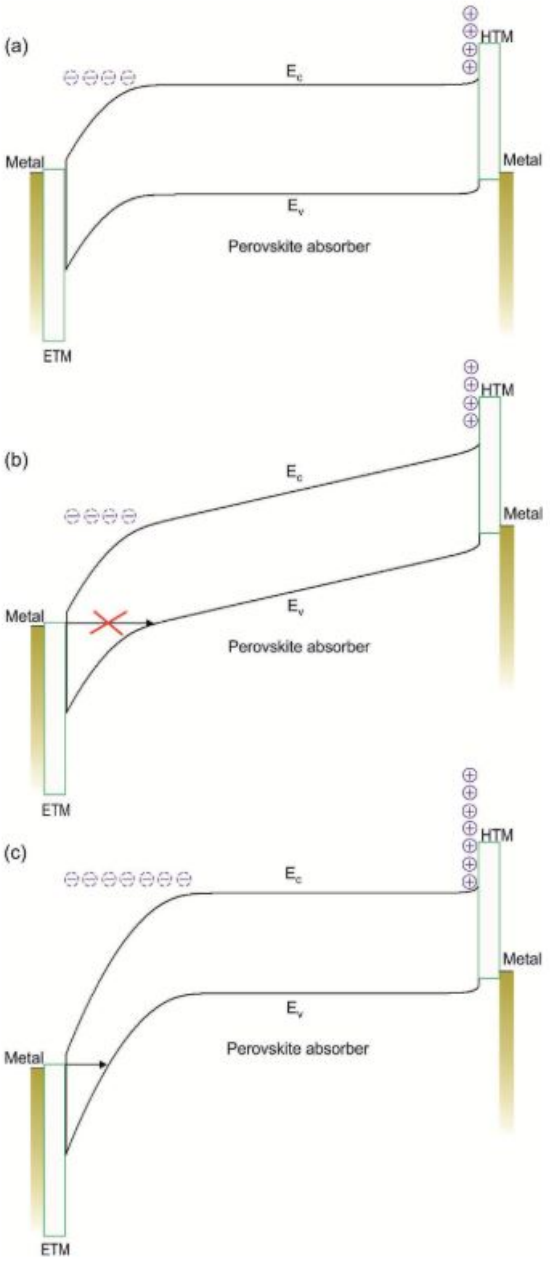


**Figure 2.11:** Band diagram indicating bending due to movement of mobile ions and charge carrier movement into the absorber layer [28]

According to the model proposed by the researchers, the reverse breakdown voltage ($V_{bd}$) is inversely proportional to the concentration of mobile ions. So, the extent and time scale of the degradation can vary depending on the composition of the perovskite absorber layer, the different transport layers, and the electrodes used for the solar cell [28]. Some studies have indicated that grain boundaries lead to band bending and increase the concentration of mobile ions, further leading to lower breakdown voltages. Also, trap sites, i.e., intermediate energy states in the bandgap, increase the probability of the tunneling effect [34] [35].

Additionally, the effect is also time-dependent, i.e., it depends on the duration of the application of the reverse bias voltage. Under extended periods, in the range of just a few minutes, the mobile ions are charge compensated by an electrochemical reaction involving oxidation or reduction. These ions would no longer be influenced by an electric field, leading to more permanent degradation, and it worsens with time and cycling. The effects are seen in the cell in lower $V_{oc}$, but further tests are necessary to obtain a more concrete understanding. For example,

studies have shown that performance can be partly recovered by maintaining the module at MPP, under light soaking, and also leaving the modules in the dark for extended periods [36] [28].

In 2020, a study on the instability of PSCs under reverse bias by Razera et. al provides additional insights into the degradation process through some visualization techniques. According to the research, the process can be divided into three different mechanisms and are briefly explained in the following sections:

### 2.7.1. Shunt formation

It has been reported that holding the PSC in reverse bias for a few minutes can lead to the formation of local shunts. The effect is more dominant in cells with metal electrodes, like gold, silver and copper. The reason is due to the migration of metal ions into the absorber layer to form filaments. These filaments are responsible for the creation of shunt or current paths within the perovskite layer. When a high current flows through these shunt paths, it can form hotspots due to energy dissipation in the form of heat as depicted in Figure 2.12.

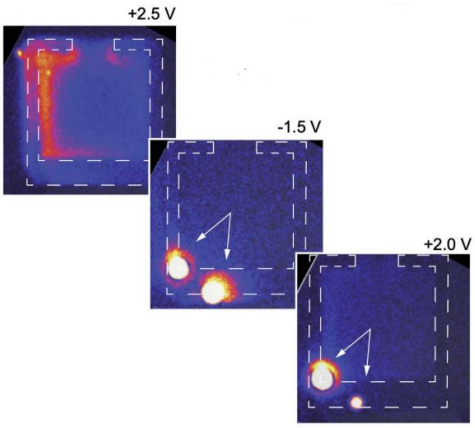


**Figure 2.12:** Hotspot formation at -1.5V and slight recovery at +2V [36]

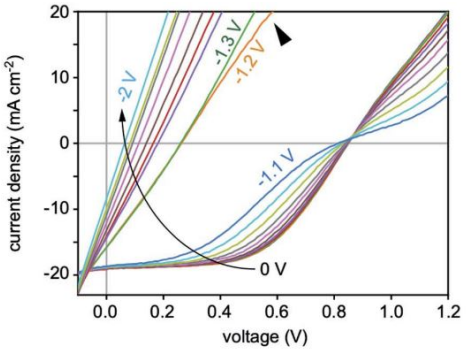


**Figure 2.13:** Shunt behavior when pre-biasing PSC at higher reverse voltages [36]

The effect is also seen in the IV plot of the PSC through a shunting behavior as illustrated in Figure 2.13 at higher negative voltages. The reverse voltage was increased progressively in steps of -0.1V for 3 minutes per step. The degradation is, however, reversible to a certain extent when a positive voltage is applied across the cell [36] [37].

### 2.7.2. S-shape development

An S-shape in the IV curve of the PSC is observed with an increase in the pre-biasing voltage as illustrated in Figure 2.14. An interesting observation in the graph is that the $V_{oc}$ remains constant, although increasing shunting behavior is noticed with an increase in the negative voltage. It indicates a process that affects charge transport but has a limited effect on recombination. A scanning transmission electron microsope (STEM) along with energy dispersive X-ray (EDX) spectroscopy tests revealed the migration of iodine towards ETL beyond LiF, and into $C_{60}$ layer when compared with an unbiased reference cell.

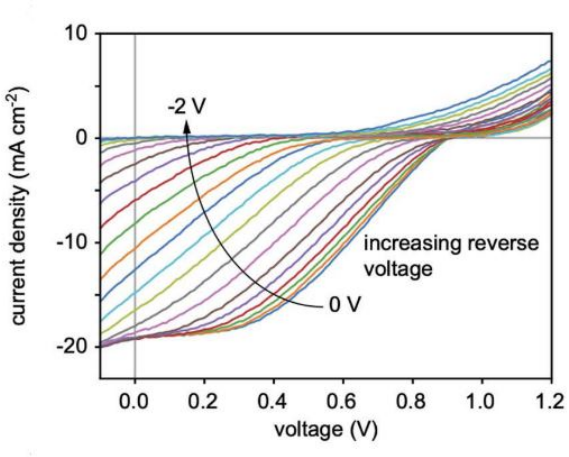


**Figure 2.14:** S-shape formation with increasing reverse voltage pre-biasing [36]

A reason cited in the study for the development of the S-shape in I-V characteristics is that iodine acts as a p-type dopant in $C_{60}$ leading to a reduction in the electric field for charge separation. It leads to lower charge carrier density, as noticed from the plot. Interestingly, the effect is reversible by maintaining the cell at a forward voltage at MPP as depicted in Figure 2.15. The cells are observed to recover when placed in the dark for one hour. The introduction of intermediate layers between the absorber layer and the ETL, like $Al_2O_3$ can prevent the leakage of iodine.

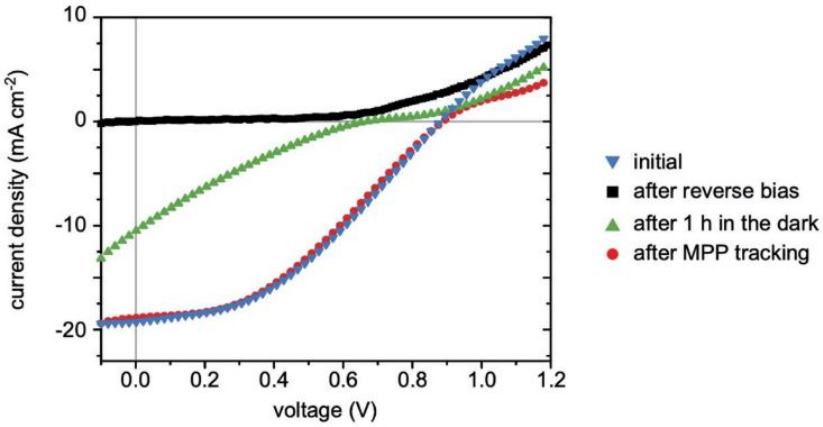


**Figure 2.15:** Improvement of module under MPP tracking [36]

### 2.7.3. Phase segregation

Lastly, the segregation of perovskites with mixed halides into iodine and bromine-rich phases is another method for the degradation of PSCs. The high current passed through the cell is suspected of introducing the phase segregation. The separation was observed using a photoluminescence (PL) test by measuring the shift in spectra from the two sides of the PSC. The reason cited is due to the carrier injection into the perovskite. Segregation in the phase leads to shorter carrier diffusion lengths. Under the PL test, the emission was shifted towards blue when illuminating from the region of high bandgap (rich in bromine) and towards red when illuminating from the low bandgap side (rich in iodine). Additionally, there is evidence of light-induced cation segregation, which mention the segregation of formamidinium and methylammonium [32]. It could be true with other cations as well.

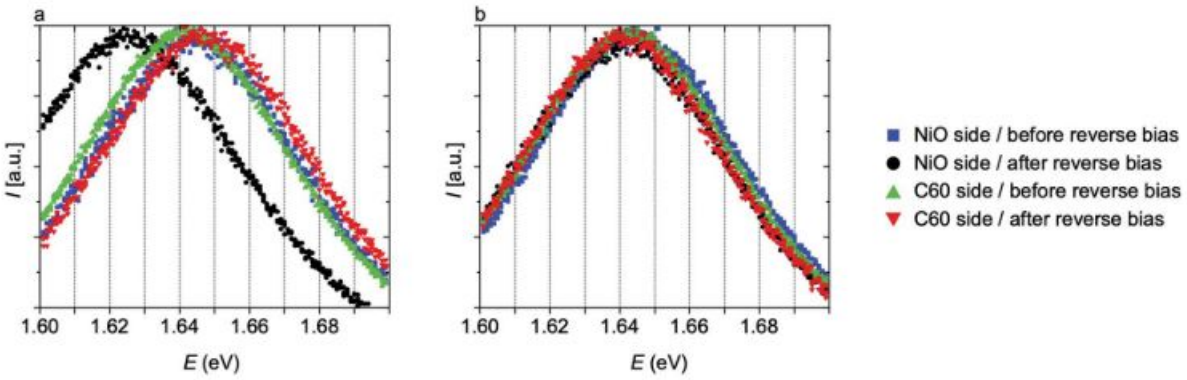


**Figure 2.16:** Phase segregation of perovskite into iodine and bromine rich layers [36]

The proposed three different mechanisms in the study can be summarised as portrayed in Figure 2.17. Depending on the composition of the perovskite, transport layers, and electrodes the dominant mechanism can vary. The figure below shows the initiation of the different mechanisms at the different negative voltages for the cell stack (n-i-p) mentioned in the figure. It is possible that the different mechanisms can play a role simultaneously, and further research is needed in this area in the coming years to address the reverse bias problem for scaling up perovskites.

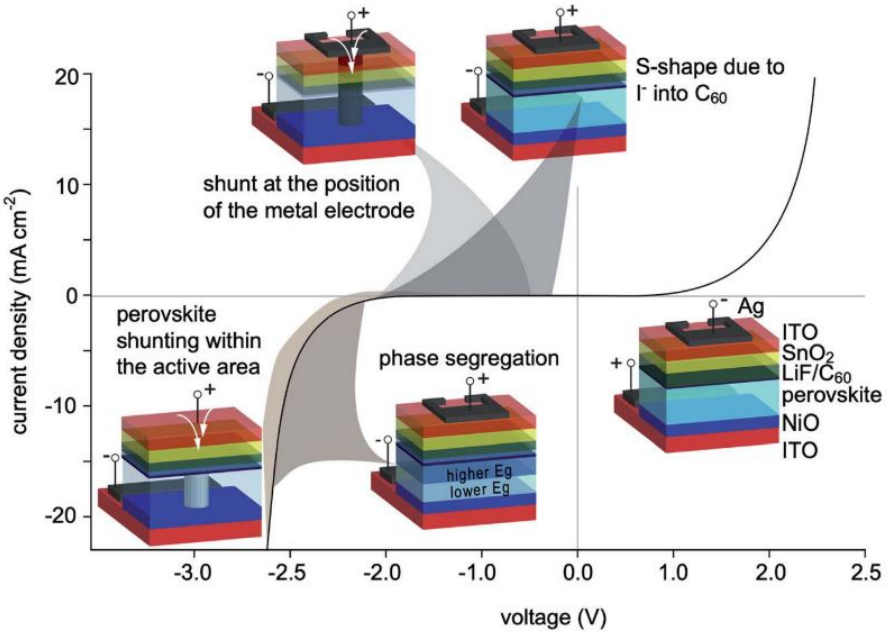


**Figure 2.17:** Summary of degradation at various reverse voltages for the mentioned cell stack [36]

# 3

# Experimental details

In this chapter, the necessary background information is provided. Perovskite mini-modules used for the experimental work are described in section 3.1. In section 3.2, the experimental setup used to perform the shading experiments is depicted. The section further includes some interesting interconnection configurations that were experimentally tested. Starting with a series connection in subsection 3.2.1 and parallel connection in subsection 3.2.2, followed by two configurations that are a combination of the two in subsection 3.2.3 and subsection 3.2.4. Finally, the effect of bypass diodes on shading is explained in section 3.3.

## 3.1. Perovskite minimodule

The perovskite stack used for the experiments follows an inverted configuration of p-i-n compared to the conventional n-i-p. In other words, the perovskite (intrinsic) layer, which absorbs the photons from the sunlight, is sandwiched between a hole transport layer (HTL) and electron transport layer (ETL) as depicted in Figure 3.1. The incoming photons encounter the HTL first. The HTL material used in the stack is nickel oxide ($NiO_x$) and ETL consists of lithium fluoride (LiF), Fullerene ($C_{60}$) and Bathocuproine (BCP). The perovskite composition used is $Cs_{0.18}FA_{0.82}PBI_{2.82}Br_{0.18}$.

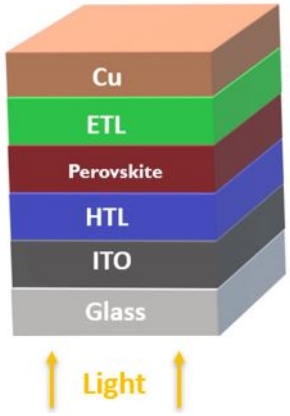


**Figure 3.1:** Different layers of the perovskite solar cell with a p-i-n configuration.

After the deposition of the different layers, the perovskite solar cell (PSC) module is laminated using poly-olefin encapsulant and a glass of 100-micron thickness, as seen in Figure 3.1. The purpose of the lamination is to protect

the deposited layers when performing experiments on the shading setup and withstand moisture ingress. A copper tape is applied at the back side of the module to create a contact between the module's terminals and the shading setup's contact pins. The contact pins are then connected to a Keithley to perform the I-V scans.

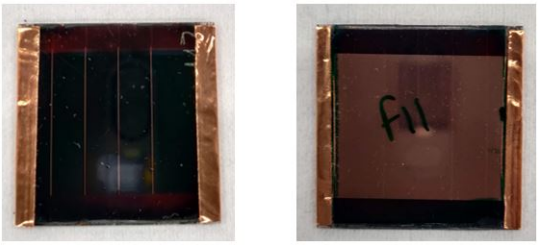

**Figure 3.2:** The front and bottom view of the laminated mini-module

| Function | Parameter |
|---|---|
| **Substrate** | 0.7 mm thick glass (3x3 $cm^2$) |
| **Lamination** | Poly-olefin with 100 micron glass |
| **Interconnection** | 4 cells series connected |
| **Active area** | 4 $cm^2$ |
| $V_{oc}$ **expected** | 4 V |
| $I_{sc}$ **expected** | 20 mA |

**Table 3.1:** Perovskite mini-module parameters

In Table 4.1, the various parameters of the module are summarised. The active area of the sample that absorbs solar energy is 4 $cm^2$. The module consists of four cells connected in series with the help of laser scribing equipment. The interconnection leads to an open circuit voltage ($V_{oc}$) of 4 volts and a short circuit current ($I_{sc}$) of about 20 mA with small variations between samples.

## 3.2. Shading setup

The experimental setup used to perform the experiments is shown in Figure 3.3. As shown, nine modules are placed in the holders, which are illuminated by a lamp calibrated to the spectrum of sunlight corresponding AM1.5 spectrum of solar irradiance [38].

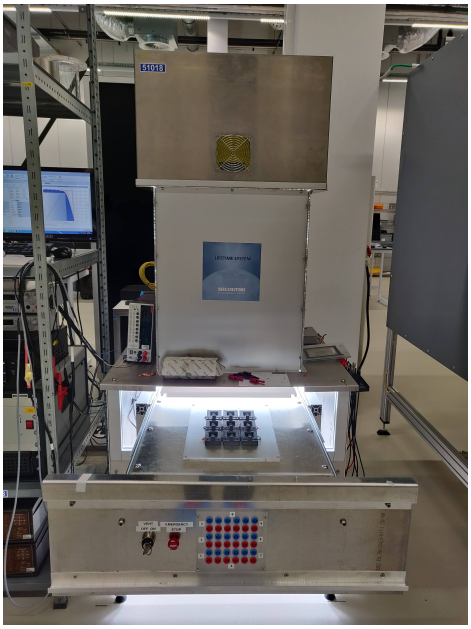

**Figure 3.3:** shading setup

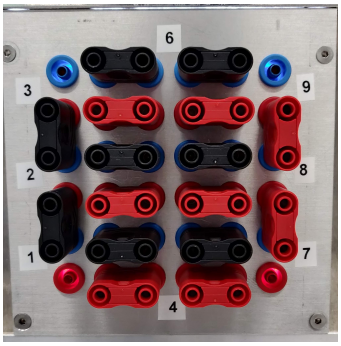


**Figure 3.4:** Total cross tied (TCT) interconnection on the shading setup

The modules are interconnected in different combinations using connectors as presented in Figure 3.4. The solar modules' positive and negative terminals are wired to the setup's front part to facilitate interconnections. The Keithley used to perform I-V scans on the interconnection uses a 4-point method with two sets of positive and

negative terminals. The two sets are connected to either end of the connection.

### 3.2.1. Series interconnection

The series interconnection of modules increases the configuration's $V_{oc}$ as shown in Figure 3.5. The blue curve represents the I-V curve for a single mini-module, and the red curve shows the resulting curve when three similar modules are connected in series, as shown in Figure 3.6. The resulting $V_{oc}$ is three times that of the single module. The configuration was simulated using Simulink.

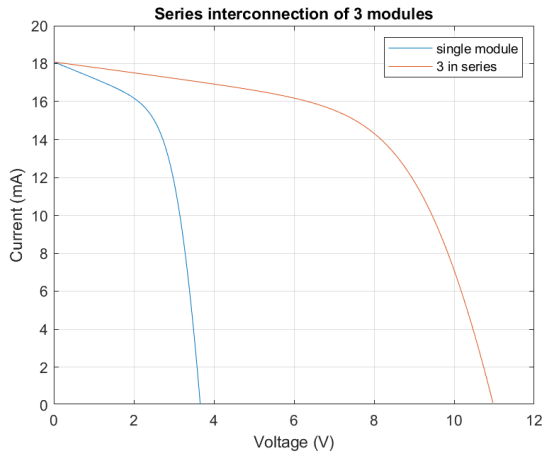


**Figure 3.5:** Plot of 3 modules in series

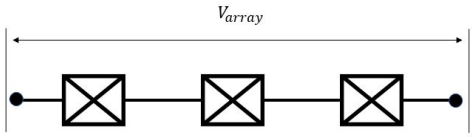


**Figure 3.6:** Series interconnection

Solar panels purchased in the market, typically employing silicon cells, usually have series interconnections between the individual cells. The primary reason is to limit the current flow and reduce the resistive losses in the circuit. Since the voltage is being summed, it also reduces the inverter losses when connected to an external grid as the voltage ratios for the transformer are lesser. So, under uniform illumination, the configuration yields optimal results. However, when a partial shade is introduced. i.e., suppose one of the mini-modules is shaded; in that case, a significant drop in the current of the overall interconnection is expected. The output current is now determined by the current produced in the shaded mini-module. It leads to the creation of reverse voltages in the shaded mini-module leading to degradation and significant loss in power.

### 3.2.2. Parallel interconnection

The parallel interconnection of the mini-modules has an opposite effect. It adds up the individual current rather than the voltage as depicted in Figure 3.7. The $I_{sc}$ of the interconnection is now three times that of the single mini-module while the $V_{oc}$ remains the same. As shown in Figure 3.8, the interconnection is realized by connecting the positive and negative terminals.

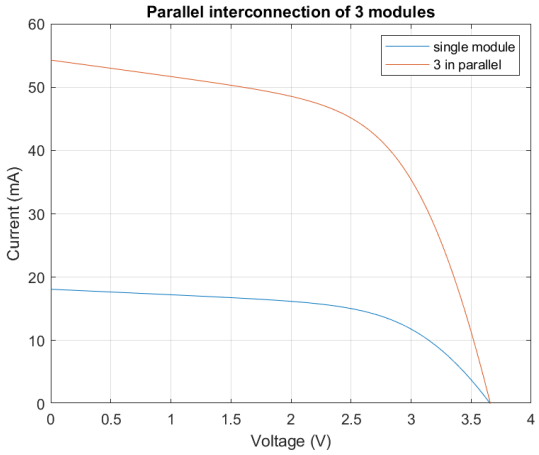


**Figure 3.7:** Plot of 3 modules in parallel

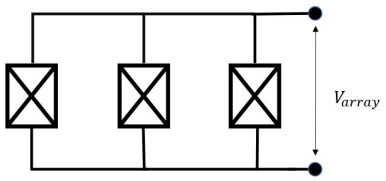


**Figure 3.8:** Parallel interconnection

There are some drawbacks to this interconnection. The increase in current leads to significantly higher resistive losses in the circuit. It further leads to a drop in power output of the array and heating up of the module itself and auxiliary components. However, a significant positive aspect of such interconnection is its better performance under partial shading. Since shading of a mini-module has a significantly lower effect on its $V_{oc}$, it does not affect the power output as significantly as observed with a series interconnection. Additionally, the shaded mini-module does not experience a reverse bias voltage that can lead to degradation.

### 3.2.3. Series-parallel interconnection

Due to the advantages and drawbacks of the series and parallel interconnections, the optimum interconnection is neither but a combination of both. One such interconnection is a series-parallel interconnection as depicted in Figure 3.10. Here, a string of mini-modules is connected in series, which are then connected in parallel with another similar string. The $V_{oc}$ is adjusted by controlling the number of mini-modules in series. In this case, as there are three in series connected in parallel with another string, it yields a $V_{oc}$ that is three times higher and doubles the $I_{sc}$. The effect can be noticed in Figure 3.9

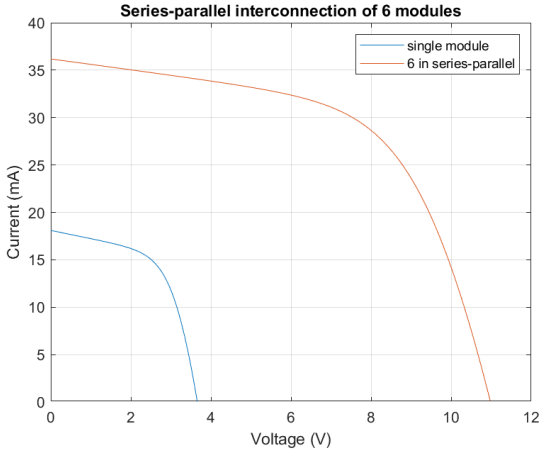


**Figure 3.9:** Plot of 6 modules in series-parallel

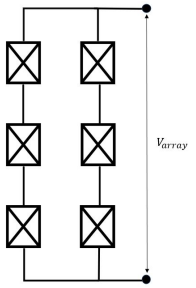


**Figure 3.10:** Series-parallel interconnection

### 3.2.4. Total cross tied interconnection

The final interconnection that is interesting to consider is the total cross-tied (TCT). In this configuration, as seen in Figure 3.12, a single row of mini-modules are connected in parallel, and the parallel connections are connected in series. Due to this, the $I_{sc}$ increases three times while the $V_{oc}$ is doubled as seen in Figure 3.11. According to the literature, experiments were conducted by other researchers mainly using silicon solar cells. The TCT configuration yielded the maximum power for the same shading conditions compared to other configurations [39] [40].

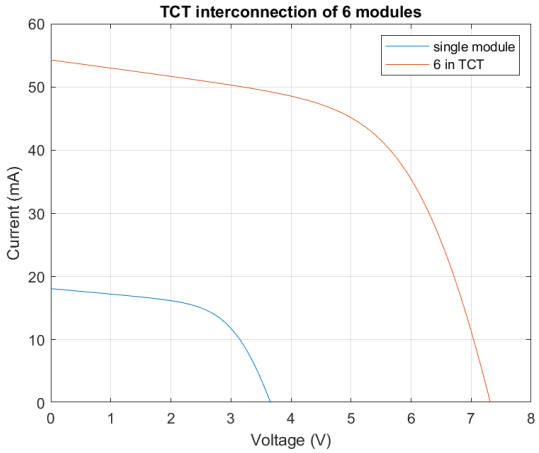


**Figure 3.11:** Plot of 6 modules in TCT

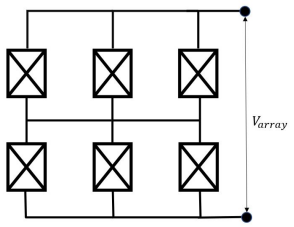


**Figure 3.12:** TCT interconnection

All the possible configurations identified earlier are plotted in a single graph for comparison in Figure 3.13. Here the effect of each configuration becomes more evident. To summarise, a series connection leads to the addition of the $V_{oc}$ while a parallel connection leads to the addition of $I_{sc}$.

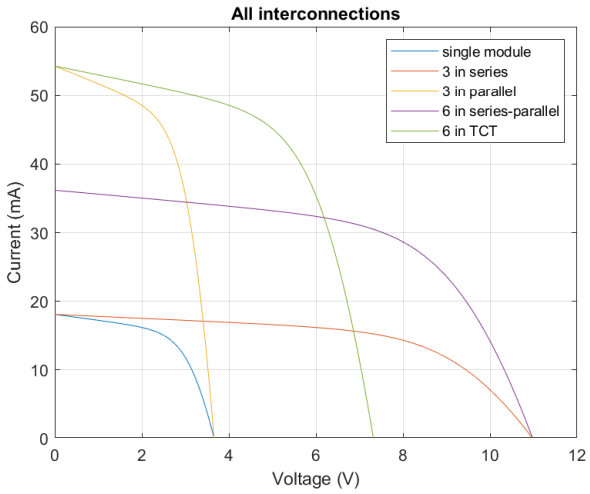


**Figure 3.13:** The different interconnection combinations compiled together

## 3.3. Bypass diodes

Bypass diodes are added to solar panels to provide an alternate path for the current to pass when there is an electrical mismatch in the performance of the PV modules. The mismatch can occur due to defects in the solar cells or, most commonly, due to partial shading of the cells. In a typical solar panel, bypass diodes are connected

across a string of series of connected cells as illustrated in Figure 3.14. It is connected in anti-parallel or reverse bias to the polarity of the solar cell, such that the diode conducts when the cell experiences a reverse bias voltage due to shading. In this way, it protects the shaded solar cells from reaching reverse breakdown voltages.

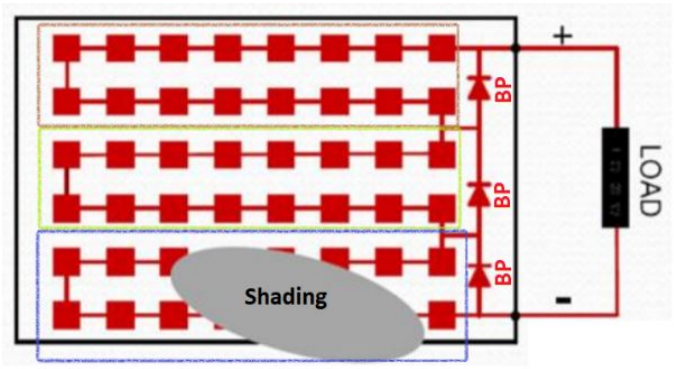


**Figure 3.14:** Bypass diodes in a solar panel [10]

The number of bypass diodes to be installed is determined by the breakdown voltage of the solar cell. The maximum number of cells connected in series for a single bypass diode is calculated using Equation 3.1. Here, $n_{max}$ is the number of cells and $V_{bd}$ is breakdown voltage. The forward voltage or the voltage at which the bypass diode gets activated is presented as $V_d$. For example, considering silicon cells with a breakdown voltage of about 13V and $V_{oc}$ of 0.5V translates to about 20 cells per bypass diode [41] [42].

$$n_{max} < \frac{V_{bd} - V_d}{V_{oc}} + 1 \tag{3.1}$$

However, if the breakdown voltages of the cell are low, then the number of bypass diodes required increases significantly, leading to higher costs in the manufacturing of the module. Another challenge brought about by bypass diodes is the creation of multiple local maxima in the output power of the solar module. It would result in complications for Maximum Power Point (MPP) trackers to track the optimum voltage for the highest possible power generation as presented in Figure 3.15 [43]. Better tracking algorithms need to be exploited, further adding to the costs. For the case of perovskites, they possess extremely low reverse bias voltages in the range of 1-4V, so it is interesting to try out other interconnection methods apart from series connection to limit the building up of reverse voltages [44].

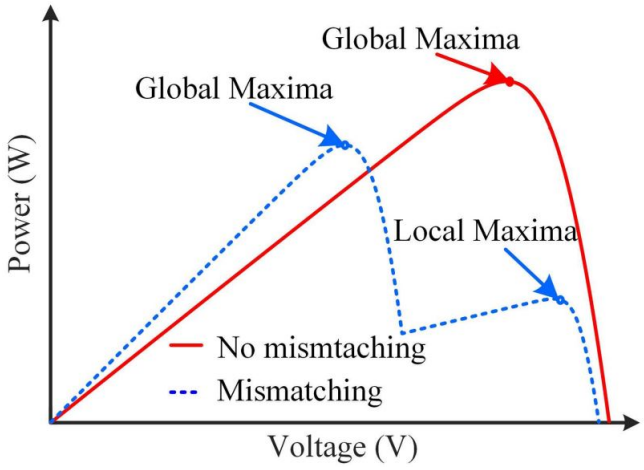


**Figure 3.15:** Creation of multiple maxima when using bypass diodes [45]

Another important consideration is the possibility of monolithic integration of bypass diodes to thin film PV modules. As already mentioned, thin film modules are fabricated using deposition techniques. Hence it is challenging to incorporate bypass diodes as it is carried out for conventional modules. It would be highly beneficial if the bypass diodes could be deposited across thin-film cells. Steim et al. discussed the prospect of printed organic bypass diodes across organic PV cells and obtained comparable results compared to conventional bypass diodes [46]. There is also evidence of incorporating bypass diodes monolithically in multi-junction cells [47]. However, the studies are over a decade old, and the odds of incorporating monolithic bypass diodes are not yet clear.

# 4

# Research methodology

This chapter will address the methodology adopted for solving the research questions. Section 4.1 discusses a brief flowchart of the steps involved in the study. In section 4.2, the multiple shading patterns that were tested is showcased. The interconnections on which the shading will be tested are mentioned in section 4.3. Finally, section 4.4 briefly introduces the Simulink model and obtaining the module parameters.

## 4.1. Methodology

The methodology for research adopted is depicted as a flowchart in Figure 4.1.

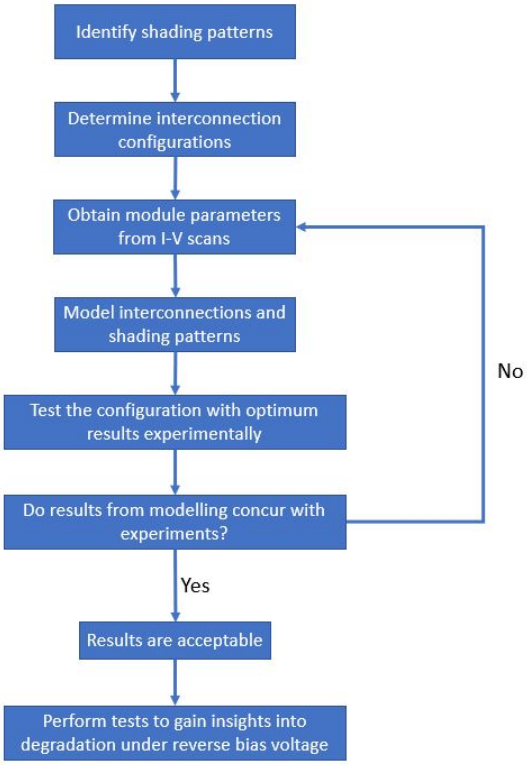


**Figure 4.1:** Research methodology

To begin with, the different patterns for shading that a solar module could experience in the outdoor environment were identified. It was followed by determining the different interconnections used conventionally and a few others based on literature. The module parameters were then obtained using a software tool to update into the Simulink model. The different interconnections and shading patterns were modelled using the PSC module parameters to obtain the configuration with the least power mismatch losses. Subsequently, the configuration with the optimal results was tested on the shading setup to check for conformance. If the results were as predicted by the model, then the results are considered acceptable. Otherwise, the model is checked, and the parameters are updated for different modules in the next set of experiments. Finally, additional tests are performed to gain insights into the degradation mechanism of the modules. The individual blocks in the flow chart are explained in detail in the upcoming sections.

## 4.2. Shading patterns

To test the effects of shading in the experimental setup, different shading patterns were identified. Literature was carefully studied to understand the patterns other researchers used for similar experiments [39] [43]. A combination of horizontal, vertical, and diagonal shading was utilised, similar to a solar panel deployed in the outdoor environment would experience. The shading patterns are showcased in Figure 4.2.

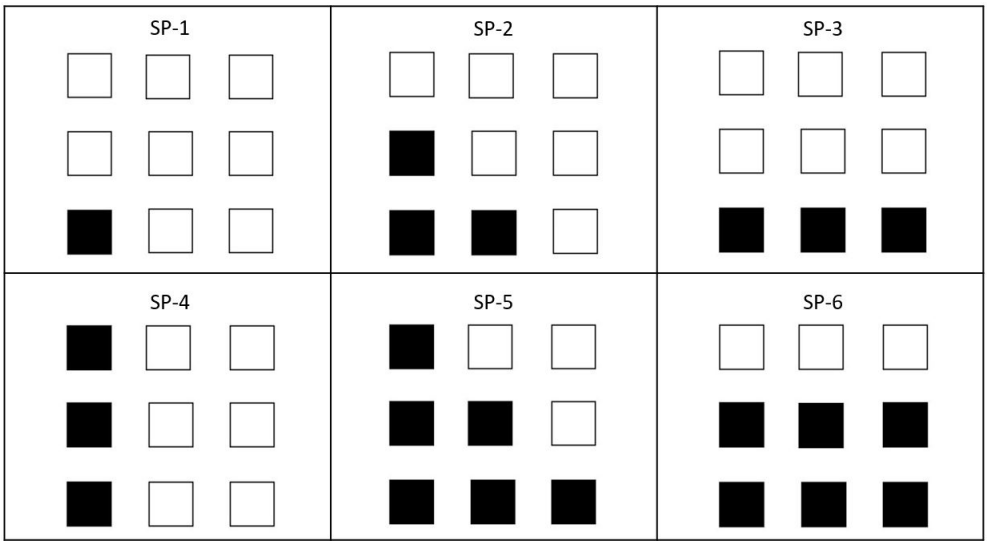


**Figure 4.2:** The different shading patterns (SP)

It must be noted here that the shading indicated in the shading patterns is complete shading of the respective module, i.e., zero illumination. Complete shading of the module leads to the worst-case scenario for the shaded modules, as it corresponds to the maximum difference in the current generated between illuminated and shaded modules. Hence, the highest possible degradation in the shaded modules due to reverse bias voltages. In outdoor conditions, the shading can be less drastic, with shading occurring between the two extremes. However, the patterns are aimed at finding the limits of the different interconnections. Each shading pattern was tested on each interconnection configuration, explained in the next section. The testing of the shading patterns on the experimental setup is showcased in Appendix A.

## 4.3. Interconnections

Based on literature study, six different interconnections were identified for study as shown in the figures below [40] [48]. Since the shading setup has the possibility of placing nine modules for performing the tests, the interconnections are accordingly determined.

The series interconnection is shown in Figure 4.3. The modules are interconnected by linking the positive and negative terminals of the adjacent modules. It builds up the output voltage, and $V_{oc}$ is equal to nine times the $V_{oc}$ of each module, assuming each module is identical. The PSC modules used for the study have a $V_{oc}$ of about 4V, leading to an interconnection $V_{oc}$ of about 36V. Also, other I-V characteristics like fill factor and $I_{sc}$ play a role. For example, the net $I_{sc}$ is determined by the module with the lowest value, so non-homogeneity in the modules can lead to a significant drop in output performance.

In Figure 4.4, the parallel interconnection is depicted. It leads to the addition of the $I_{sc}$ to nine times of each module (about 180 mA). This interconnection method is more tolerant to mismatch in the performance of the individual modules, either due to fabrication or partial shading. However, the building up of current and resulting low voltage leads to high resistive losses (heat) and voltage transformers to step up the voltage, as mentioned in Appendix F. Thus, due to the shortcomings of the series and parallel interconnections, a combination of both will be investigated to find a more optimal point for partial shading conditions.

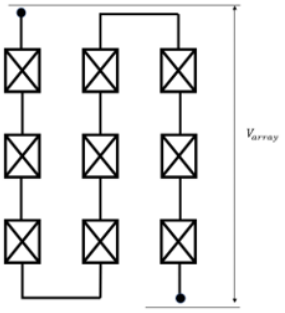


**Figure 4.3:** Series interconnection

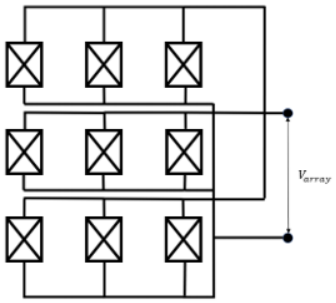


**Figure 4.4:** Parallel interconnection

Correspondingly, a series-parallel and total cross tied (TCT) were also tested, illustrated in Figure 4.5 and Figure 4.6. In both cases, the configurations will have a similar $V_{oc}$ and $I_{sc}$ of three times that of a single module. However, they will perform significantly differently under partial shading conditions as observed in the respective mismatch losses.

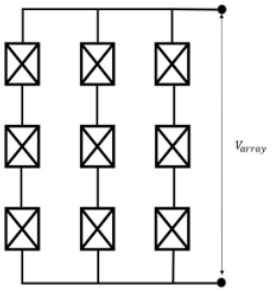


**Figure 4.5:** Series-parallel interconnection

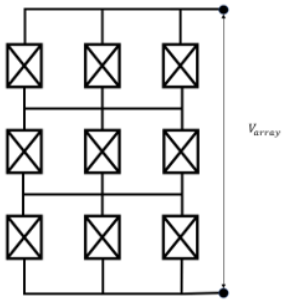


**Figure 4.6:** Total cross tied (TCT) interconnection

Additionally, as mentioned earlier bypass diodes are used in solar modules as a mitigation strategy to partial shading. So, it is interesting to understand its effect on interconnections. For this purpose, TCT and series interconnection are chosen, as depicted in Figure 4.7 and Figure 4.8 respectively. The reason for choosing TCT is that, according to literature, it is expected to perform the best, so it is interesting to understand the improvement by adding bypass diodes [49]. Finally, the series connection was chosen because it is typically how the interconnections are made in solar panels and would act as a reference point. The incorporation of bypass diodes in the experimental in briefly discussed in Appendix C.

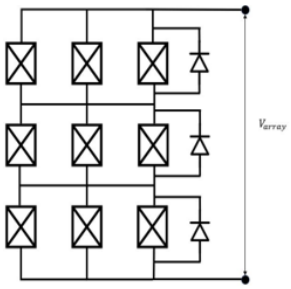

**Figure 4.7:** TCT interconnection with bypass diodes

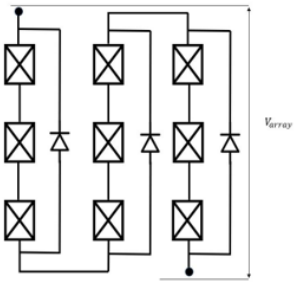

**Figure 4.8:** Series interconnection with bypass diodes

The above interconnections under full illumination are plotted to give an idea of their behavior in Figure 4.9.

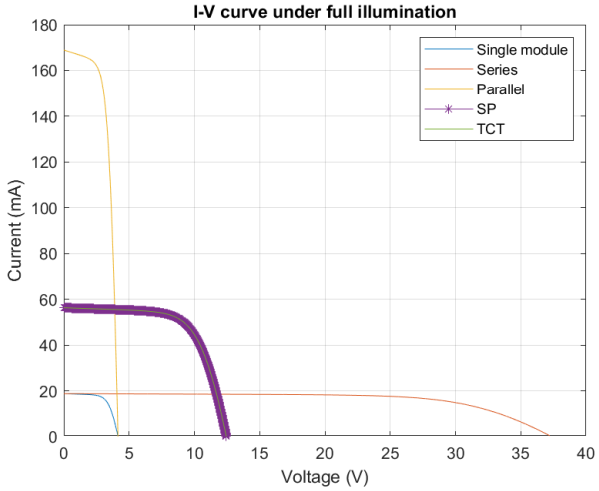


**Figure 4.9:** IV full illumination

## 4.4. Modelling

The Simulink model used for the simulation purpose is presented in Appendix B. The model uses a single diode equivalent solar cell circuit which requires parameters to be input to simulate a solar module similar to the one used in experimentation. The different parameters are depicted in Table 4.1.

The parameters were obtained using a curve fit tool called ”IV fit”. The tool works by iteratively changing the value of the parameters in the solar cell circuit equation (Equation 2.2) to obtain a set of parameters that can resemble the IV characteristics of that of the mini-module. As illustrated in Figure 4.8, the parameters generated from the tool closely represent the IV curve obtained from the tests. Also, all the nine modules utilized for the experiments were unidentical, as shown in Figure 5.8. Hence, a mini-module with the average performance of all in terms of efficiency was chosen as representative for all modules. In other words, although the experiments utilize non-identical modules, the simulation uses a single representative set of parameters for all nine modules.

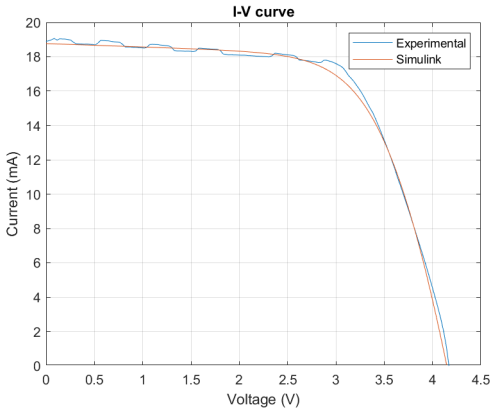


**Figure 4.10:** Curve fitting

| Parameter | Value |
|---|---|
| Reverse saturation current ($I_0$) | $2.58 * 10^{-8}$ A |
| Shunt resistance ($R_{sh}$) | 5112.5 ohms |
| Series resistance ($R_s$) | 19.5 ohms |
| Ideality factor ($n$) | 3 |
| Photocurrent ($I_{ph}$) | 18.9 mA |

**Table 4.1:** Perovskite module parameters

The ideality factor presented in Table 4.1 is not indicative of the actual value for PSCs. The value presented in other studies mention it be about 1.3 [50]. The increase in ideality factor presented here is due to the degradation of the module after lamination. Therefore, the curve fit tool that was utilised to obtain the parameters indicates a higher value to fit the curve. However, the ideality factor is not of much consequence to the results from the model.

# 5

# Results

The results obtained in the research are analyzed in this chapter. In section 5.1, shading tests are performed for a single module for a deeper understanding of the behavior, with two orientations of shading in subsection 5.1.1 and subsection 5.1.2. The modeling results are reviewed in section 5.2. The shading experiment is briefly discussed in section 5.3. Lastly, a comparison is made between the model and experiments in section 5.4 to understand the model's accuracy in predicting the behavior.

## 5.1. Shading a single mini-module

Initially, a subset of the interconnection configuration was tested to gain a preliminary understanding. For example, three modules were connected in series and parallel, and one of them was shading one of them to see if the expected results were obtained. Surprisingly at that stage, it was noticed that shaded modules in a series interconnection were degrading instantly. Therefore, it was necessary to develop a deeper understanding of the consequence of shading at the module level before trying out the different interconnections. Consequently, two different shading patterns were performed, perpendicular and parallel to laser interconnection scribes.

### 5.1.1. Perpendicular shading

The shading of the single module is conducted as shown in Figure 5.1. In this case, all the individual cells are equally shaded, i.e., the shaded area is the same. Since each of the cells experience an equal amount of irradiance, they produce the same amount of current.

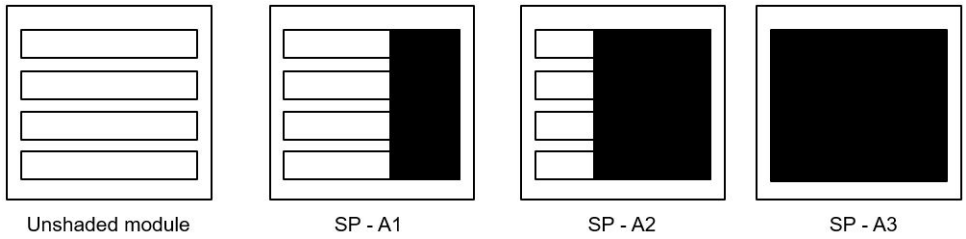


**Figure 5.1:** Perpendicular shading patterns (SP)

As the shading is increased from SP-A1 to SP-A3, the short circuit current decreases proportionally, as illustrated in Figure 5.2. When the module is completely shaded, it produces no current, and the curve immediately goes in

the negative direction. Notably, the test led to no degradation in the module as the IV scan was performed after removing the shading. The reason is that no reverse bias voltage is built-up across any of the cells as the current generated in each cell is equal. It also reaffirms that the unequal current generation in series connected cells leads to reverse voltages across cells producing less current.

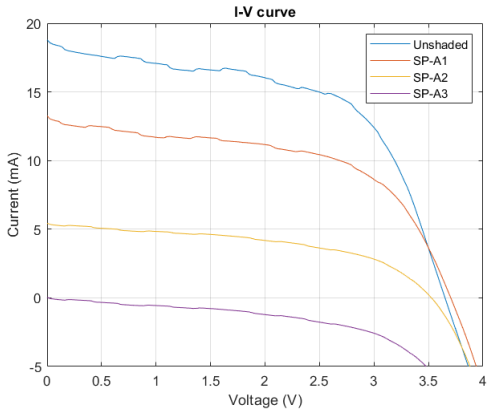


**Figure 5.2:** Perpendicular shading graph

### 5.1.2. Parallel shading

The shading pattern is changed in the scenario of parallel shading. The cells were shaded entirely, as seen in Figure 5.3. Each shading case leads to the building of reverse bias voltage across the shaded cells. The magnitude of the reverse bias voltage across the shaded cells increases as we shift from SP-B1 toward SP-B3. This is because more energy generated in the illuminated cells needs to be dissipated in the shaded cells. Hence it leads to a high reverse voltage at short circuit condition. Each cell's $V_{oc}$ is about 1V, and the reverse bias voltage in the SP-B3 condition at the short circuit condition would be about 3V. In contrast, SP-B1 and SP-B2 would lead to a voltage of -0.3V and -1V, respectively.

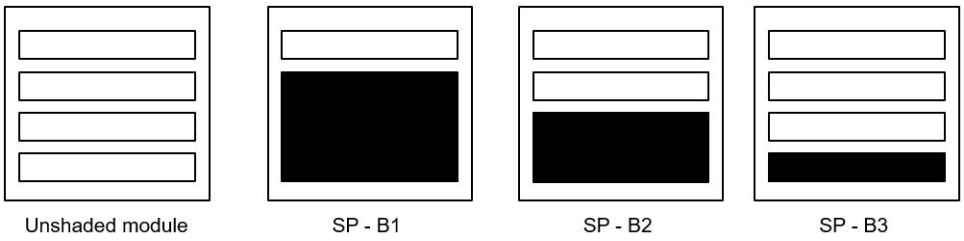


**Figure 5.3:** Parallel shading patterns (SP)

The reverse bias voltages across the shaded cells degrade the module. It was observed in the I-V scan after the removal of the shade. Figure 5.4 shows the I-V curve while the module is shaded, and Figure 5.5 depicts the scan after the shade is removed to check for degradation. After SP-B1, the module regains its initial performance. However, SP-B2 shading leads to much higher $I_{sc}$ than expected, signifying the shaded cells have potentially reached their respective breakdown voltages and started conducting in the reverse bias condition. It is confirmed when a forward scan of the module is performed after the shade is removed. The $V_{oc}$ drops to about 2.7V from 3.7V. The effect worsens with SP-B3 as the module degrades further to a $V_{oc}$ of 1.2V.

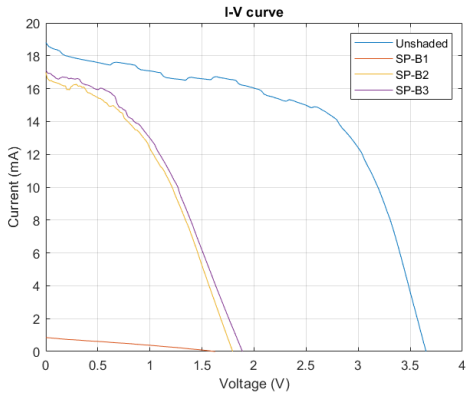


**Figure 5.4:** Parallel shading

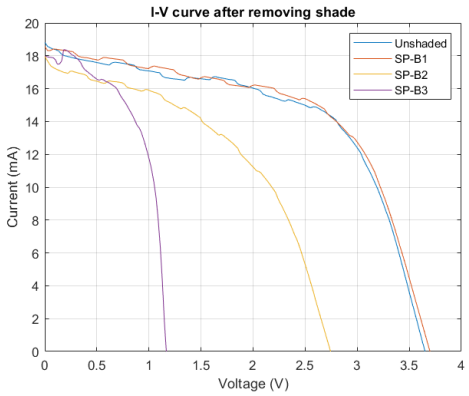


**Figure 5.5:** After the removal of shade

The test provides insight into the reverse bias behavior of PSCs and confirms the low reverse breakdown voltage mentioned in literature [28] [36]. Consequently, it is apparent that it is impossible to perform all the tests for each of the interconnection configurations due to the limited availability of the PSC modules. Hence, the interconnections were modeled to better understand the configuration's performance without damaging many modules.

## 5.2. Modelling results

The model built in Simulink tests the different interconnection configurations owing to the shading patterns. However, some assumptions involved in the model may not completely represent the actual experiments, and they are as follows:

- The solar cell parameters indicate only the forward bias characteristics of the module. It was not possible to append the reverse bias characteristics like the reverse bias breakdown voltage in the model. By default, the model considers the reverse breakdown voltage of the cell to be equal to that of Silicon at 18V.
- The model does not consider any resistance in the circuit. Resistive losses can influence the mismatch losses in configurations involving high current.
- Lastly, no losses due to voltage stepping up and down are considered. It can be critical when the voltage step-up ratios are high as it can lead to high transformer losses.

The voltage across the shaded cells at the short-circuit, MPP and open-circuit is depicted in Appendix D. It is shown that voltages reach higher than 18V in negative bias across the shaded cell in series connection. However, this is not likely to happen if tested because the breakdown voltage of PSC module is significantly lower and the shaded module would degrade. This is due to the first assumption pointed out above. The model predicts the performance of the different interconnections but the degradation of the modules is not built into it.

The power mismatch loss is the difference in the amount of power that can be potentially captured and that is actually retrieved for the given interconnection configuration with a shading pattern. It is represented as follows:

$$MML\% = \frac{Power_{recoverable} - Power_{recovered}}{Power_{recoverable}} * 100 \tag{5.1}$$

The recoverable power depends on the number of illuminated modules (representated as $N_{illum}$) in the specific shading patterns. It is calculated by multiplying the power at MPP ($P_{MPP}$) for the representative module and the number of illuminated modules as shown Equation 5.2. The $P_{MPP}$ for the representative module is equal to **51 mW**. For example, for SP-1, the $N_{illum}$ equals 8, as so many modules are illuminated.

$$P_{recoverable} = N_{illum} * P_{MPP} \tag{5.2}$$

The output current and voltage parameters are obtained from the Simulink model, which is then processed in Matlab to calculate the mismatch losses. The mismatch losses for each interconnection and shading pattern combination are illustrated in Figure 5.6. Lower mismatch losses are desirable as it signifies that a smaller proportion of the power is lost for that interconnection.

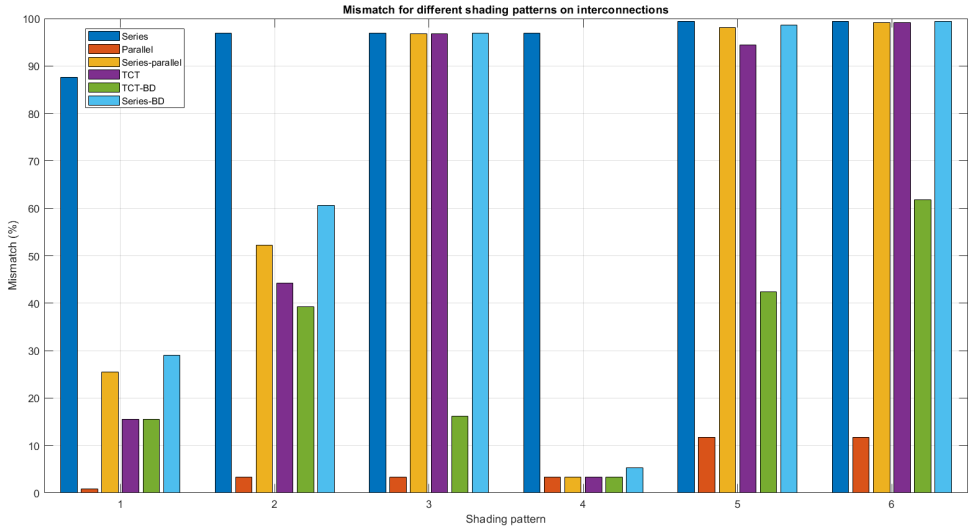


**Figure 5.6:** Mismatch losses of interconnections at different shading patterns

Some key takeaways from the above bar chart are:

- Series interconnection has the highest power losses for all the shading patterns. It is expected as the shaded cells limit the current in all the modules leading to a significant drop in overall power.
- The other configurations apart from series are more resilient to shading in the vertical direction, as seen with SP-4 in the figure.
- Parallel interconnection appears to have the least mismatch losses. The assumptions and limitations in the model mentioned earlier contribute to this, which will be explained further.

To understand the variability of power with respect to increasing resistance, a variable resistor was incorporated into the model. The resistance symbolizes the resistance in the interconnections, intermediate cabling, and other resistive losses. It can be seen from Figure 5.7 that a parallel interconnection has significantly higher power losses with an increase in the resistance compared to a series or a TCT configuration. It is a direct consequence of the high current in this configuration, as power loss is a function of the second order of current ($P_{loss} = I^2 * R$). The current in the parallel interconnection is nine and three times higher compared to series and TCT configuration, respectively. Additionally, low voltage build-up in a parallel configuration leads to high transformer losses due to low voltage ratios. The inverter losses are explained further in Appendix F.

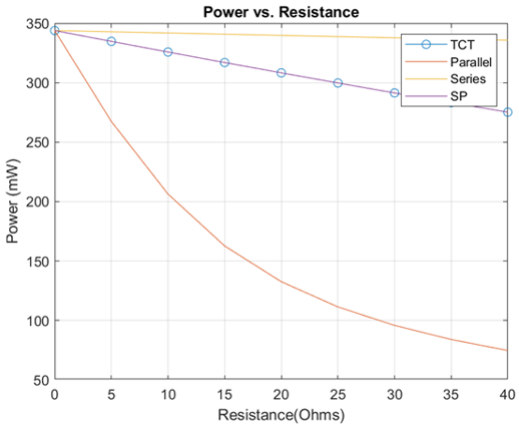


**Figure 5.7:** Power output as a function of resistance for the different interconnection configurations

Due to the above reasons, TCT interconnection with bypass diodes, as illustrated in Figure 4.7 is considered the optimal configuration for partial shading. Furthermore, the configuration was tested experimentally to check the model's accuracy in predicting the mismatch losses.

## 5.3. Experiments

Nine modules were used to perform the shading tests. However, the modules were not identical, as seen from the I-V plots of the nine modules in Figure 5.8. The modules were observed to degrade after lamination. The reason is suspected to be due to the high temperature of 130°C required to melt the encapsulant material. As perovskites are highly sensitive to temperature, high temperature in the laminator degrades the perovskite layer and possibly changes the structural and chemical composition of the PSC [37]. The degradation of the modules due to lamination is further elaborated in Appendix E.

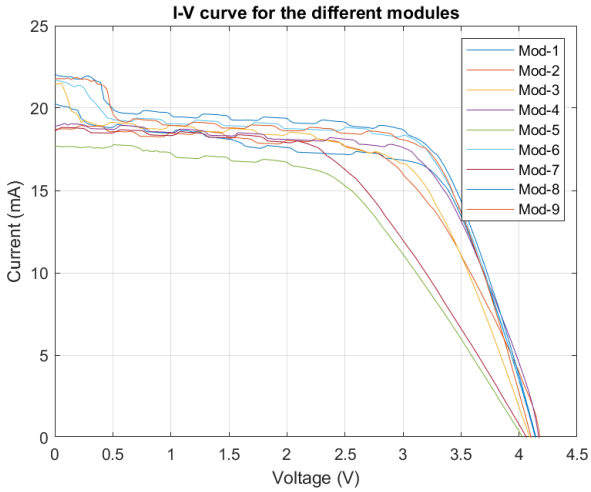


**Figure 5.8:** The nine mini-modules used for experiments

The electrical parameters of the different modules used for experiments are tabulated in Table 5.1.

| Module | Isc (mA) | Voc (V) | Fill factor (%) | Efficiency (%) |
|---|---|---|---|---|
| 1 | 20.3 | 4.1 | 62.6 | 13.1 |
| 2 | 18.7 | 4.2 | 61.6 | 12.1 |
| 3 | 21.5 | 4.1 | 56.8 | 12.5 |
| 4 | 18.9 | 4.2 | 67.7 | 13.3 |
| 5 | 17.7 | 4.1 | 53.4 | 9.6 |
| 6 | 21.7 | 4.2 | 62.0 | 14.0 |
| 7 | 18.6 | 4.1 | 53.6 | 10.2 |
| 8 | 22.1 | 4.2 | 61.8 | 14.2 |
| 9 | 21.8 | 4.1 | 62.6 | 14.0 |

**Table 5.1:** Electrical parameters of the modules utilised for shading experiments

The nine modules were placed in the different holders in the shading setup. Since TCT interconnection with bypass diodes was chosen as the optimal interconnection based on the simulation results, it was tested on the setup. Once the modules were placed in the holders, they were exposed to irradiation from the lamp. IV scans were conducted to obtain the data. In the next section, the conformity of the simulation and experimental results is discussed.

## 5.4. Comparison between model and experiments

In this section, the results from the experiments are plotted along with the simulation results. Figure 5.9 depicts the plot of TCT configuration with bypass diodes when all the modules are illuminated fully. The experiment shows higher shunting behavior than the simulation and higher series resistance. It is due to non-homogeneity in the modules used for the experiment and some modules having low fill factors like modules 5 and 7.

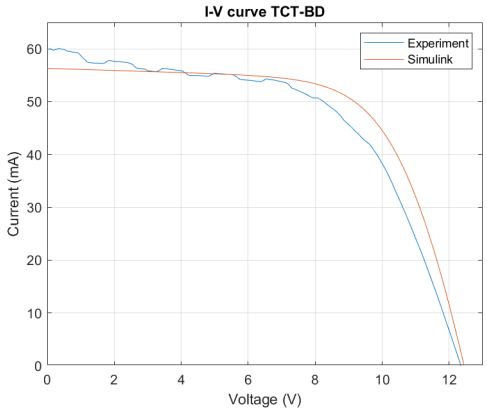


**Figure 5.9:** TCT with bypass diodes under full illumination

In Figure 5.10, the plot is shown for the shading condition, SP-1. The activation of the bypass diode is seen here in the form of a step in the curve. The bypass diode connected to the bottom row of parallel connected modules in the TCT interconnection is activated due to the mismatch in current with the above two rows. The short circuit current in the last row is about 40 mA, while the above two rows generate 60 mA leading to the plot shown in the figure.

In contrast, two steps in the curve are noticed in Figure 5.11. This is because each row in the TCT interconnection generates different current levels. The top row generates $3{*}I_{sc}$ ($\approx$ 60 mA), the middle row $2{*}I_{sc}$ ($\approx$ 40 mA), and the bottom row produces $I_{sc}$ same as that of a single module. The short circuit current is a multiple of the number of illuminated modules for each row.

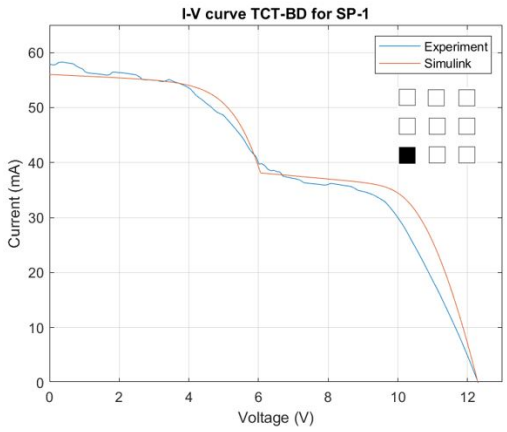


**Figure 5.10:** Shading pattern 1

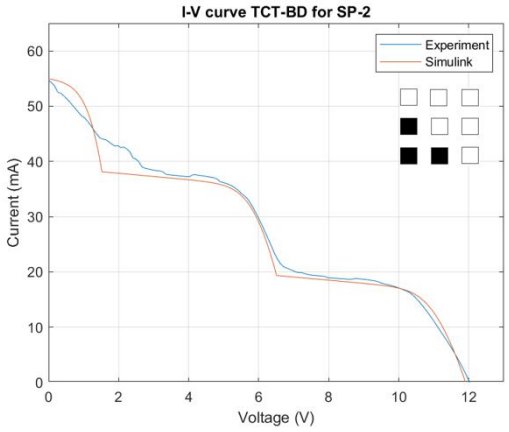


**Figure 5.11:** Shading pattern 2

Alternatively, no step is observed in the plot in Figure 5.12. It is because the last row is completely shaded in this shading type. Therefore, the diode bypasses the entire row as no current is generated in any of the modules. Hence, the $V_{oc}$ is doubled as only two rows contribute to the voltage.

There is just a single step in the plot in Figure 5.13. One of the columns is entirely shaded, leading to an equal circuit current in each row of the interconnection. Due to no mismatch in the current between the different rows, the bypass diodes are not activated in this case. The short circuit current is equal to two times that of a single module as only two modules are illuminated in each row.

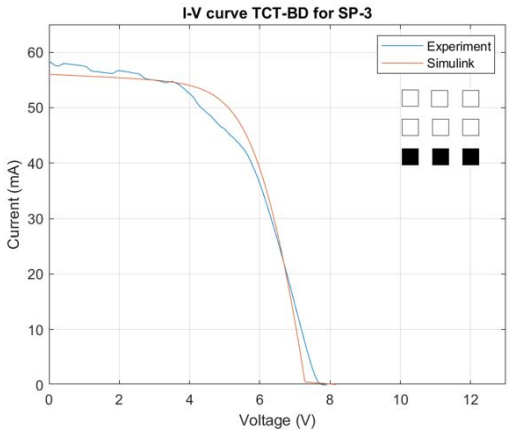


**Figure 5.12:** Shading pattern 3

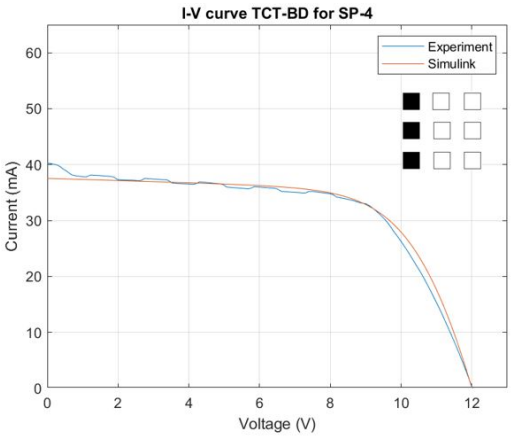


**Figure 5.13:** Shading pattern 4

A single step in the plot is observed in the SP-5 shading condition as depicted in Figure 5.14. The bottom row is completely shaded, so it is bypassed. Only the first and the second rows have illuminated modules. Also, since the bottom row is entirely shaded, the $V_{oc}$ reduces as well.

Finally, In the last shading condition, SP-6, two rows of the interconnection are shaded. As only one row of modules produces power, it is similar as if three modules were in parallel, and the resulting plot is depicted in Figure 5.15.

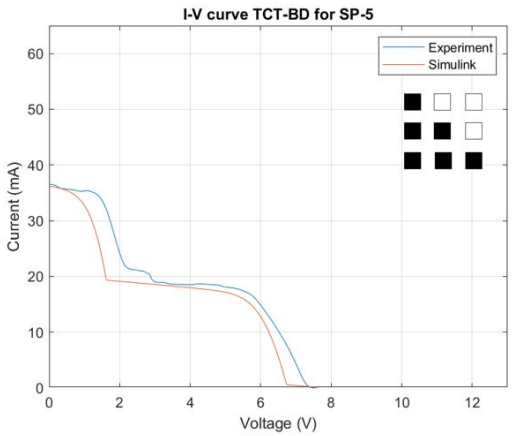


**Figure 5.14:** Shading pattern 5

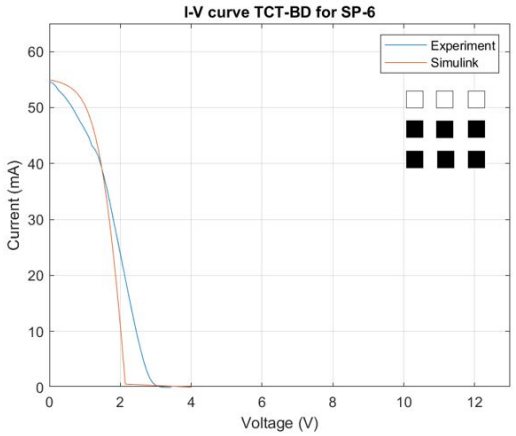


**Figure 5.15:** Shading pattern 6

# 6

# Additional tests

Few additional tests were conducted for a deeper insight into shading behavior of PSCs. Firstly, an electroluminescence test was performed to visualize the degradation in the module, which is discussed in section 6.1. In section 6.2, the module was exposed to reverse bias voltage to understand its breakdown limit. The recovery of the module after a breakdown is tested in section 6.3. Lastly, the semi-transparent modules are tested to understand its response to shading in section 6.4.

## 6.1. Electroluminescence test

Electroluminescence (EL) is a phenomenon of light emission from a crystal exposed to external electric voltage or current [51]. The EL of PV cells are typically conducted to understand the integrity of the cell. The integrity includes micro-cracks, ruptures in the metal grids, and shunts between base and emitter. Researchers have also used EL for more advanced measurements like determining the diffusion length of charge carriers, carrier collection length, junction voltage, and series resistance of a PV cell [52] [53]. For this study, the EL test was conducted primarily to look for shunting behavior between the cells and degradation of the cells when exposed to parallel shading, as discussed in subsection 5.1.2.

The test was conducted in a dark room to reduce the interference of any external radiation on the results as the emission intensity is low. The module is connected to a constant voltage source with the functionality of controlling the applied voltage in the experimental instrument. The voltage was varied in the proximity of the module's open circuit voltage to check for light emission. Since the PV module was in the dark, it behaves like a typical diode following the characteristics discussed in Figure 2.5. The PV module begins to emit radiation when the voltage equals the $V_{oc}$, which is captured by the camera.

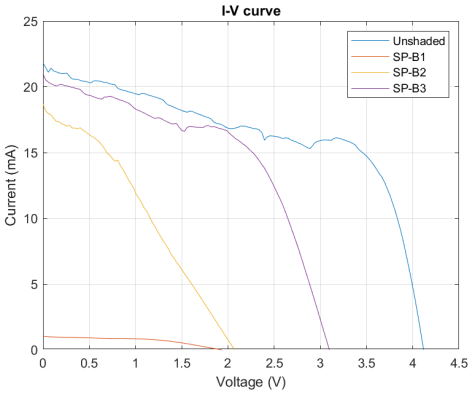


**Figure 6.1:** Parallel shading

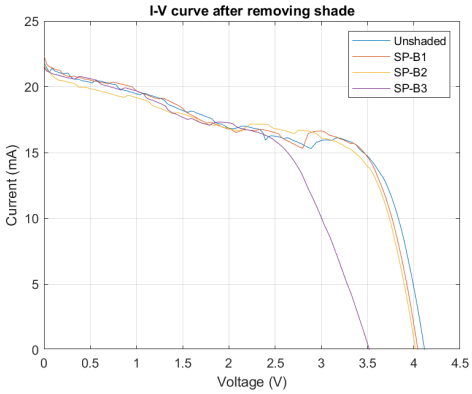


**Figure 6.2:** After removing shade

The IV characteristics of the module are shown in the plots above. Figure 6.1 shows the IV plot for the different shading conditions. The measurement after the shading was removed to check for degradation is depicted in Figure 6.2. It was observed that when the module experiences SP-B3 shading, there is degradation in the module with a drop in the $V_{oc}$. Since the shading leads to the highest reverse voltages across the shaded cell, it leads to its degradation. It is interesting to see the degradation with the help of EL test. However, it must be noted that the module before shading tests was already heavily shunted and was of lower quality. Due to the shunting property, there was no degradation seen in SP-B2, as was expected from the earlier perpendicular shading test. Unfortunately, the test could not be repeated with better modules due to the unavailability of the EL test equipment.

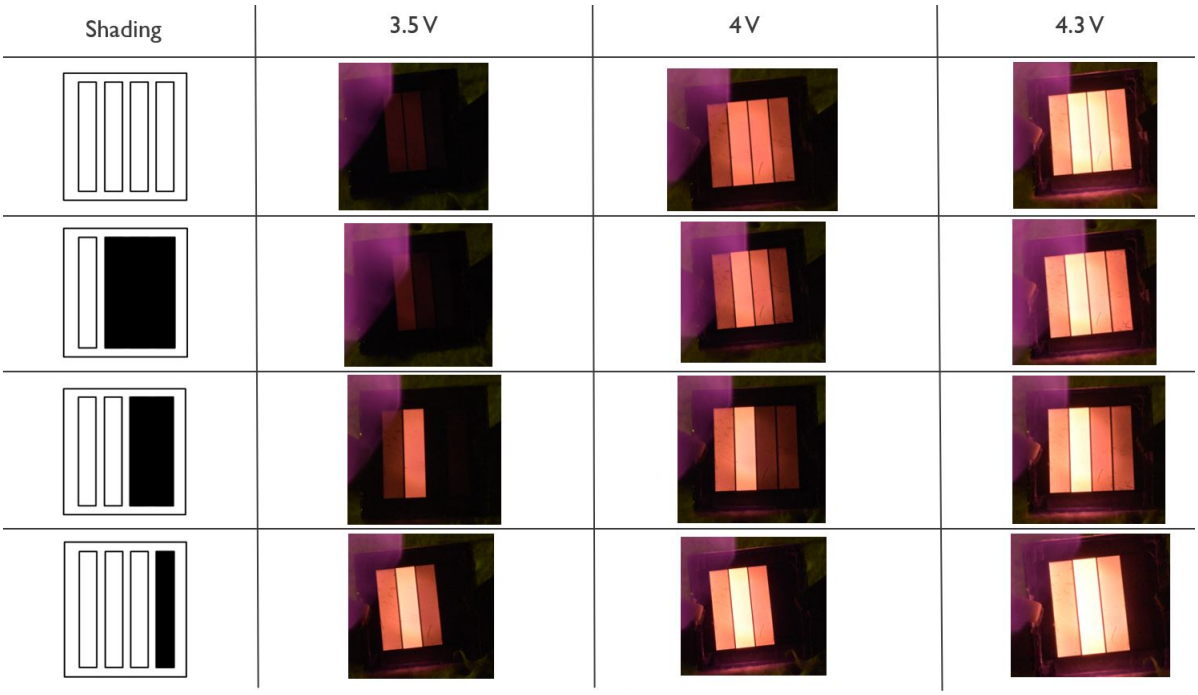


**Figure 6.3:** EL test images at different parallel shading conditions

As illustrated in Figure 6.3, the EL test was conducted before shading the module and after each shading instance. The voltage across the module was varied between 3.5V and 4.3V to check for light emission. Some critical observations from the test are as follows:

- Before the application of shading on the module, all the cells in the module light up at 4V as it is equal to the

module's $V_{oc}$. However, not all the cells light up equally well, suggesting that the module was degraded. As the voltage is increased across the module, the intensity of illumination increases as more energy is dissipated in the form of light at higher voltages.

- At shading SP-B1, the results are similar to the previous case. No degradation is expected due to reverse voltages in the range of only 0.3V across the shaded cells.
- The second shading scenario of SP-B2 produces different results. Interestingly, the unshaded cells begin to illuminate at 3.5V, and the shaded cells appear to be slightly degraded when observing the illumination at 4V. All the cells light up at higher voltage, but the shaded cells illuminate at a lower intensity. It must be noted that at this shading instance, there was no degradation observed in the IV plot. The lower illumination of the shaded cells is indicative of the slight degradation in the shaded cells due to ion movement which is likely reversible if the module is exposed to forward bias voltage.
- Lastly, in the third shading case of SP-B3 the degradation in the shaded cell is evident. The unshaded cells also illuminate at 3.5V; this is due to the module's drop in $V_{oc}$ to 3.5V as depicted in Figure 6.2. However, at higher voltages, the shaded cell does not illuminate, confirming the degradation noticed from the IV scan.

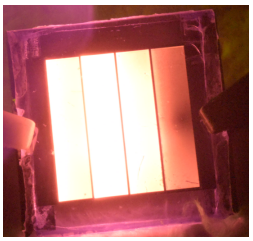

**Figure 6.4:** EL test at 5V

Furthermore, the applied voltage across the module was increased further to 5V. The intensity of illumination increases at higher voltages. Interestingly, the right-most cell also lights up, and a dark spot is observed in the left-most cell. An explanation for this is the formation of defects within the perovskite absorber layer at reverse bias voltages due to ion movement, which is leading to degradation of the cell. As indicated from literature in subsection 2.7.1, there could be hotspot creation due to the migration of copper atoms into absorber layer leading to the degradation of the cell. It is clear that the reverse biased cell is degrading, but more tests are needed to find the root cause.

## 6.2. Reverse bias breakdown

The module was stressed in reverse bias to understand the breakdown voltage of the module. As seen from Figure 6.5, the breakdown voltage is about -6.5V. However, the voltage is not for the cell but for the four-cell series interconnected module. For a single cell, it would be the module breakdown voltage divided by four, equal to about -1.6V.

As reported from the literature, the breakdown is in the range of -1 and -4V. It is low for a PSC module to be deployed outdoors. The degradation can damage the module entirely; however, a part of the performance can be recovered, which will be elaborated on in the next section.

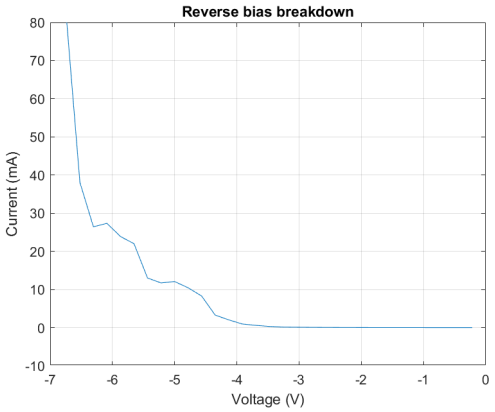


**Figure 6.5:** Reverse bias breakdown

## 6.3. Recovery from breakdown

The module that experienced reverse breakdown was light soaked for a period of one hour. Interestingly, the module recovered a part of its performance with time when exposed to light, as illustrated in Figure 6.6. The light soaking reverses some of the effects of breakdown caused by the movement of mobile ions.

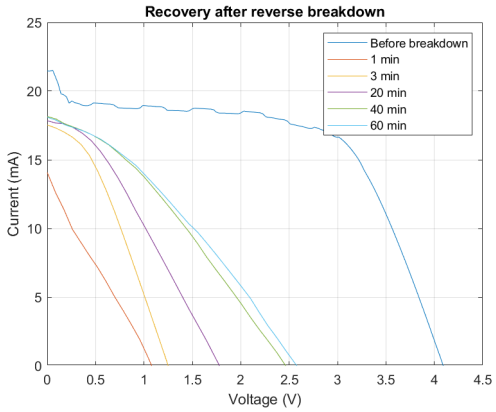


**Figure 6.6:** Recovery after reverse bias breakdown

However, the recovery is marginal and the module shows high shunting. It is interesting to carry out further tests, like placing it in dark for extended periods to see the recovery and also perform MPP tracking tests to check for potential recovery. Due to the constraints of time, it was not possible carry out these tests but it would help to provide additional insights about the behavior.

## 6.4. Shading of semi-transparent modules

The parallel shading test described in subsection 5.1.2 was conducted on semi-transparent modules that did not use copper as the electrode but Indium Tin Oxide (ITO). The module had seven cells interconnected in series compared to four cells in the earlier modules. Due to this, six shading patterns were possible, beginning with shading six cells and ending with shading a single cell. Figure 6.7 shows the IV scan at each shading instance, and Figure 6.8 depicts the module's performance after each shading instance under full illumination.

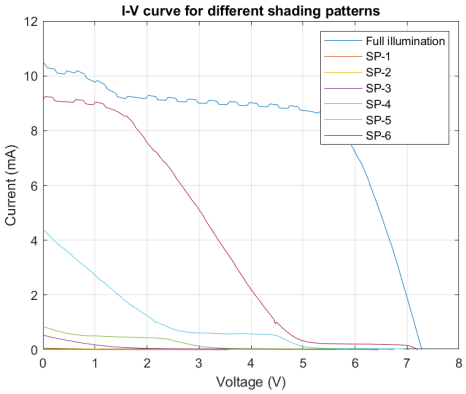


**Figure 6.7:** Under parallel shading

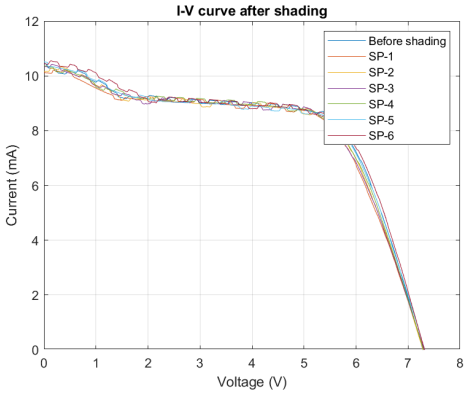


**Figure 6.8:** After removing shade

As the shading is reduced, the current in the module increases. It signifies that the shaded modules are conducting at reverse bias voltage. But, it is clear that after the shade is removed, the module has not degraded. The ability to conduct in reverse bias and not degrade is a desirable property because that means that cell can behave as a bypass diode when shaded. But, another alternate explanation for the observed effect could be the possibility of alternate paths for the current to pass which does not lead to the degradation of the absorber layer. More extensive tests that stress the cells to higher reverse bias voltages are needed to further understand the cause.

# 7

# Conclusion and outlook

The thesis aimed to understand the behavior of PSCs to shading and to test the possibility of alternate interconnections to improve shade tolerance. Section 7.1 concludes the research by looking at the answers to the posed research questions. Finally, section 7.2 presents recommendations for future research.

## 7.1. Conclusion

Shading is an essential aspect of PV technology to be satisfied for outdoor deployment. Six different interconnections and shading patterns were chosen at the start of the thesis project and were modeled using Simulink and Matlab software. From earlier shading tests, the poor reverse bias characteristics of perovskites were evident, so it was clear that it would not be feasible to test all the interconnections on the shading setup. Therefore, the interconnections were modeled and aided in developing a more in-depth understanding of the response of the interconnections to shading. Due to the assumptions and limitations of the model, parallel interconnection had the least mismatch losses. However, considering resistance and inverter losses in the analysis, TCT shows better performance with additional gains with the introduction of bypass diodes.

Additionally, experimental tests were conducted on the shading setup with the optimal interconnection. The purpose was to validate the simulation results. The experiments yielded results close to the simulation; notably, no degradation was noticed in any modules as predicted by the model. This was because the shaded modules did not experience a reverse bias voltage large enough to cause deterioration. It also proved that mismatch losses predicted from the model for the other interconnections were acceptable.

Furthermore, other tests were conducted to understand the reverse bias characteristics of perovskites. Shading tests were conducted on a single module to verify that the degradation induced in the modules was due to reverse bias voltage. Then, an electroluminescence test helped to visualize the degradation. It proved that the module was deteriorating under partial shading by showing the creation of dark spots; likely caused as a consequence of a hotspot on the shaded cell when exposed to the most severe shading condition. Reverse bias tests were conducted to see the breakdown limit of the modules. The module broke down at -6.5V, leading to a cell breakdown voltage of about -1.6V. Interestingly, the degradation was partly recoverable when exposed to light for one hour, but the complete performance was not regained. The reason for the low breakdown voltage of the module can be suspected to be due to the copper electrodes, as other studies by researchers mention the migration of metal atoms into the absorber layer to create shunt paths. Furthermore, the semi-transparent modules demonstrated a higher breakdown voltage likely benefiting from the use of ITO as the electrode rather than copper.

To conclude, the project's objective was to understand the behavior of perovskites to partial shade and the potential of alternative interconnections to reduce its effects. As the shading tests were conducted, the weak reverse bias

properties of the material became evident, and the research was directed towards obtaining insights into the behavior. Furthermore, the conclusions achieved in this study highlights that more studies on the behavior of perovskites under shading are needed for the rapid scaling-up of the technology in the coming years.

## 7.2. Outlook

The section provides some recommendations for future study to understand the shading behavior of perovskites better and a few solutions that can be implemented:

**Simple modifications to laser scribing:** Currently, the cells' scribing is performed so that it is horizontal to the ground when installed. Wolf et. al. proposes a simple solution of having the scribing vertical instead as it can reduce the reverse bias stresses on the cells. Shading in the field can occur due to many external elements, like dirt, snow, or debris, which is uniformly distributed across a solar panel. However, certain kinds of shading from adjacent panels or materials that can accumulate at the bottom, like during snowfall, induce a particular type of shading. The shading is horizontal to the ground and concentrated at the bottom of the panel. So having vertical scribes avoids the creation of a current differential in the cells and hence avoids building up of reverse bias stress [54]. Also, Lan et. al. proposes a solution of additional laser scribes to divide the long cells in series into parallel interconnections. In this manner, the cells are no longer connected in series. However, a series-parallel connection is established, which leads to significantly better performance under partial shading, as seen from the mismatch losses in Figure 5.6 [55].

**More extensive shading tests:** In this study, the shading was performed for only a single IV scan. The response to shading over extended periods and at different illumination levels must be tested, as that would be more representative of the outdoor conditions. The PSC modules could perform differently under such conditions, which needs to be better understood. Also, TCT and series-parallel interconnections that are proposed in this study can be implemented through laser scribing and verified if the respective response to shading is similar to that predicted by this study.

**Lamination:** The lamination method for the PSC modules in this study involved poly-olefin as the encapsulant. For the lamination process, temperatures of 130°C were reached. With PSCs known to degrade at 85°C, the lamination was seen to deteriorate the module significantly. Therefore other techniques of lamination that employ lower temperatures are necessary. Similar challenges exist for organic light emitting diodes (OLEDs), and other researchers have proposed some solutions. One is to use low-temperature gas barrier films by atomic layer deposition where the process happens at 80°C [56]. Another is a low-temperature plastic lamination process proposed by Guo et. al. where the process happens at 60°C [57]. However, the processes needed to adapt for PSCs and the feasibility needs to be studied further.

**Avoid metal electrodes:** Copper metal electrodes were used in the module that was tested for this study. Metal electrodes provide benefits like low resistance to the flow of current and in turn, better electrical parameters. But, metals are known to migrate into the absorber layer leading to shunting the cell. Other electrodes like ITO were tested in the study, providing better resilience to reverse bias voltages. Another interesting research study published recently proposes using carbon-based electrodes to achieve reverse bias voltages of 9V. The PSC modules with these electrodes also passed the "hotspot" test described by the IEC [33].

**Passivation layers:** Introducing passivation layers at the interface of the transport layers, and the absorber layer could be beneficial towards achieving better reverse bias properties. Passivation of grain boundaries is seen as an effective method to minimize ion migration. Some materials like $Al_2O_3$ and PCBM are investigated to promote the reduction of ion migration [36]. Chen et. al. provides an extensive range of passivation materials that could be tested [58]. However, the investigation is primarily focused on improving the forward bias, not reverse bias parameters. It would be interesting if similar passivation techniques could also improve the reverse bias properties of PSCs.

**Monolithic integration of bypass diodes:** From the study it is clear that bypass diodes need to be used to improve the shade tolerance of PSCs. However, the fabrication of PSC is different from silicon; it uses deposition tech-

niques to create interconnections between the cells. So, it would be more desirable to have fabrication techniques that allow for the deposition of bypass diodes onto the substrate. It would immensely reduce the complications in incorporating the diodes and improve feasibility.

# Bibliography


[1] Usenobong F Akpan and Godwin E Akpan. "The Contribution of Energy Consumption to Climate Change: A Feasible Policy Direction". In: *International Journal of Energy Economics and Policy* 2 (1 2012), pp. 21–33. ISSN: 2146-4553. URL: www.econjournals.com.

[2] *Energy and climate change*. May 2021. URL: https://www.eea.europa.eu/signals/signals-2017/articles/energy-and-climate-change.

[3] *Global CO2 emissions have been flat for a decade*. Nov. 2021. URL: https://www.carbonbrief.org/global-co2-emissions-have-been-flat-for-a-decade-new-data-reveals.

[4] Fraunhofer ISE. *Photovoltaics report*. 2022. URL: https://www.ise.fraunhofer.de/content/dam/ise/de/documents/publications/studies/Photovoltaics-Report.pdf (visited on 08/20/2022).

[5] The Renewable Energy Hub. *History of Solar PV*. URL: https://www.renewableenergyhub.co.uk/main/solar-panels/the-history-of-solar-power/ (visited on 06/20/2022).

[6] Adolf Goetzberger, Christopher Hebling, and Hans-Werner Schock. *Photovoltaic materials, history, status and outlook*. 2003.

[7] The Nobel prize. *Albert Einstein*. URL: https://www.nobelprize.org/prizes/physics/1921/einstein/facts/.

[8] Stephen Klassen. "The Photoelectric Effect: Reconstructing the Story for the Physics Classroom". In: *Science and Education* 20.7 (2011), pp. 719–731. ISSN: 09267220. DOI: 10.1007/s11191-009-9214-6.

[9] Nokia Bell Labs. *Bell Labs' Greatest Innovations*. URL: https://www.bell-labs.com/about/history/. (accessed: 25.06.2022).

[10] Ricardo A. Marques Lameirinhas, João Paulo N. Torres, and João P. de Melo Cunha. *A Photovoltaic Technology Review: History, Fundamentals and Applications*. Mar. 2022. DOI: 10.3390/en15051823.

[11] Wikipedia. *International Space Station*. URL: https://en.wikipedia.org/wiki/International_Space_Station. (accessed: 05.07.2022).

[12] NREL. *Best Research-Cell Efficiency Chart*. 2022. URL: https://www.nrel.gov/pv/cell-efficiency.html (visited on 08/08/2022).

[13] Bruno Ehrler et al. "Photovoltaics reaching for the shockley-queisser limit". In: *ACS Energy Letters* 5 (9 Sept. 2020), pp. 3029–3033. ISSN: 23808195. DOI: 10.1021/acsenergylett.0c01790.

[14] Matthew T. Boyd et al. "Evaluation and validation of equivalent circuit photovoltaic solar cell performance models". In: *Journal of Solar Energy Engineering, Transactions of the ASME* 133.2 (2011). ISSN: 01996231. DOI: 10.1115/1.4003584.

[15] E. L. Meyer. "Extraction of Saturation Current and Ideality Factor from Measuring Voc and Isc of Photovoltaic Modules". In: *International Journal of Photoenergy* 2017 (2017). ISSN: 1687529X. DOI: 10.1155/2017/8479487.

[16] Raoul Weegink. *Challenge the future Next Generation Shade-Tolerant Reconfigurable PV Modules for Urban Landscapes Graduation Project*. Tech. rep. URL: www.repository.tudelft.nl/..

[17] Arno HM Smets et al. *Solar Energy: The physics and engineering of photovoltaic conversion, technologies and systems*. UIT Cambridge, 2015.

[18] E. M.G. Rodrigues et al. "Simulation of a solar cell considering single-diode equivalent circuit model". In: *Renewable Energy and Power Quality Journal* 1.9 (May 2011), pp. 369–373. ISSN: 2172038X. DOI: 10.24084/repqj09.339.

[19] Practical EE. *Diode*. URL: https://practicalee.com/diodes/. (accessed: 08.07.2022).

[20] João Paulo N. Torres et al. “The effect of shading on photovoltaic solar panels”. In: *Energy Systems* 9 (1 Feb. 2018), pp. 195–208. ISSN: 18683975. DOI: 10.1007/s12667-016-0225-5.

[21] Marc De Graef and Michael E McHenry. *Structure of materials: an introduction to crystallography, diffraction and symmetry*. Cambridge University Press, 2012.

[22] Peng Gao, Michael Grätzel, and Mohammad K. Nazeeruddin. *Organohalide lead perovskites for photovoltaic applications*. 2014. DOI: 10.1039/c4ee00942h.

[23] Martin A. Green, Anita Ho-Baillie, and Henry J. Snaith. *The emergence of perovskite solar cells*. 2014. DOI: 10.1038/nphoton.2014.134.

[24] Mohammed Istafaul Haque Ansari, Ahsanulhaq Qurashi, and Mohammad Khaja Nazeeruddin. *Frontiers, opportunities, and challenges in perovskite solar cells: A critical review*. June 2018. DOI: 10.1016/j.jphotochemrev.2017.11.002.

[25] Shiro Kawachi et al. “Structural and Thermal Properties in Formamidinium and Cs-Mixed Lead Halides”. In: *The Journal of Physical Chemistry Letters* 10.22 (2019). PMID: 31645099, pp. 6967–6972. DOI: 10.1021/acs.jpclett.9b02750. eprint: https://doi.org/10.1021/acs.jpclett.9b02750. URL: https://doi.org/10.1021/acs.jpclett.9b02750.

[26] Michael Grätzel. *The light and shade of perovskite solar cells*. Tech. rep. 2014. URL: www.nature.com/naturematerials.

[27] Juan Pablo Correa-Baena et al. “The rapid evolution of highly efficient perovskite solar cells”. In: *Energy and Environmental Science* 10.3 (Mar. 2017), pp. 710–727. ISSN: 17545706. DOI: 10.1039/c6ee03397k.

[28] Andrea R. Bowring et al. “Reverse Bias Behavior of Halide Perovskite Solar Cells”. In: *Advanced Energy Materials* 8.8 (Mar. 2018). ISSN: 16146840. DOI: 10.1002/aenm.201702365.

[29] Alessandro Senocrate et al. “The nature of ion conduction in methylammonium lead iodide: a multimethod approach”. In: *Angewandte Chemie International Edition* 56.27 (2017), pp. 7755–7759.

[30] Heejae Lee et al. “Direct Experimental Evidence of Halide Ionic Migration under Bias in CH3NH3PbI3–x Cl x-Based Perovskite Solar Cells Using GD-OES Analysis”. In: *ACS Energy Letters* 2.4 (2017), pp. 943–949.

[31] Simon Min Sze. *Semiconductor devices: physics and technology*. John wiley & sons, 2008.

[32] Caleb C. Boyd et al. *Understanding Degradation Mechanisms and Improving Stability of Perovskite Photovoltaics*. Mar. 2019. DOI: 10.1021/acs.chemrev.8b00336.

[33] Dmitry Bogachuk et al. “Perovskite Photovoltaic Devices with Carbon-Based Electrodes Withstanding Reverse-Bias Voltages up to –9 V and Surpassing IEC 61215:2016 International Standard”. In: *Solar RRL* 6.3 (Mar. 2022). ISSN: 2367198X. DOI: 10.1002/solr.202100527.

[34] Yongbo Yuan and Jinsong Huang. “Ion migration in organometal trihalide perovskite and its impact on photovoltaic efficiency and stability”. In: *Accounts of chemical research* 49.2 (2016), pp. 286–293.

[35] Jiang-Jun Li et al. “Microscopic investigation of grain boundaries in organolead halide perovskite solar cells”. In: *ACS applied materials & interfaces* 7.51 (2015), pp. 28518–28523.

[36] Ricardo A.Z. Razera et al. “Instability of p-i-n perovskite solar cells under reverse bias”. In: *Journal of Materials Chemistry A* 8.1 (Jan. 2020), pp. 242–250. ISSN: 20507496. DOI: 10.1039/c9ta12032g.

[37] Leyla Najafi et al. “Reverse-Bias and Temperature Behaviors of Perovskite Solar Cells at Extended Voltage Range”. In: *ACS Applied Energy Materials* 5.2 (Feb. 2022), pp. 1378–1384. ISSN: 25740962. DOI: 10.1021/acsaem.1c03206.

[38] NREL. *Reference Air Mass 1.5 Spectra*. 2022. URL: https://www.nrel.gov/grid/solar-resource/spectra-am1.5.html (visited on 08/12/2022).

[39] Ahmed Al Mansur and Ruhul Amin. “Performance Investigation of Different PV Array Configurations at Partial Shading Condition for Maximum Power Output”. In: *2019 International Conference on Sustainable Technologies for Industry 4.0 (STI)* 0.Ld (2019), pp. 1–5.

[40] G. Sai Krishna and Tukaram Moger. “Investigation of Power losses on Solar Photovoltaic Array Interconnections Under Mismatch Conditions”. In: *Technology and Economics of Smart Grids and Sustainable Energy* 6.1 (Dec. 2021). ISSN: 21994706. DOI: 10.1007/s40866-021-00117-8.

[41] Jan Bauer et al. “Physical mechanisms of electrical breakdown in silicon solar cells”. In: *Annual report of Max Planck Institute of Microstructure Physics* (Oct. 2009), pp. 44–45.

[42] Romênia G. Vieira et al. *A comprehensive review on bypass diode application on photovoltaic modules*. May 2020. DOI: 10.3390/en13102472.

[43] Dhanup S. Pillai et al. “Design and testing of two phase array reconfiguration procedure for maximizing power in solar PV systems under partial shade conditions (PSC)”. In: *Energy Conversion and Management* 178 (Dec. 2018), pp. 92–110. ISSN: 01968904. DOI: 10.1016/j.enconman.2018.10.020.

[44] Narendra Shiradkar et al. “Effect of shading on the switching of bypass diodes in PV modules”. In: *Reliability of Photovoltaic Cells, Modules, Components, and Systems VII*. Vol. 9179. SPIE, Oct. 2014, p. 91790C. ISBN: 9781628412062. DOI: 10.1117/12.2062470.

[45] Kamran Ali Khan Niazi, Yongheng Yang, and Dezso Sera. “Review of mismatch mitigation techniques for PV modules”. In: *IET Renewable Power Generation* 13.12 (2019), pp. 2035–2050. ISSN: 17521424. DOI: 10.1049/iet-rpg.2019.0153.

[46] Roland Steim et al. “Flexible polymer photovoltaic modules with incorporated organic bypass diodes to address module shading effects”. In: *Solar Energy Materials and Solar Cells* 93.11 (2009), pp. 1963–1967. ISSN: 09270248. DOI: 10.1016/j.solmat.2009.07.013. URL: http://dx.doi.org/10.1016/j.solmat.2009.07.013.

[47] M. Stan et al. “Design and performance of high efficiency III-V space solar cells with monolithic bypass diode architecture”. In: *Conference Record of the 2006 IEEE 4th World Conference on Photovoltaic Energy Conversion, WCPEC-4* 2 (2006), pp. 1865–1868. DOI: 10.1109/WCPEC.2006.279858.

[48] Paula dos Santos Vicente et al. “Shading position effects on photovoltaic panel output power”. In: *International Transactions on Electrical Energy Systems* 30.1 (Jan. 2020). ISSN: 20507038. DOI: 10.1002/2050-7038.12163.

[49] Rupendra Pachauri et al. “Experimental analysis to extract maximum power from PV array reconfiguration under partial shading conditions”. In: *Engineering Science and Technology, an International Journal* 22.1 (Feb. 2019), pp. 109–130. ISSN: 22150986. DOI: 10.1016/j.jestch.2017.11.013.

[50] Pietro Caprioglio et al. “On the Origin of the Ideality Factor in Perovskite Solar Cells”. In: *Advanced Energy Materials* 10.27 (2020), pp. 1–9. ISSN: 16146840. DOI: 10.1002/aenm.202000502.

[51] Heinz K Henisch. “Electroluminescence”. In: *Reports on Progress in Physics* 27.1 (1964), p. 369.

[52] Torben Potthoff et al. “Detection of the voltage distribution in photovoltaic modules by electroluminescence imaging”. In: *Progress in Photovoltaics: Research and Applications* 18.2 (2010), pp. 100–106. ISSN: 10627995. DOI: 10.1002/pip.941.

[53] Daniela Fontani et al. “Electroluminescence test to investigate the humidity effect on solar cells operation”. In: *Energies* 11.10 (2018), pp. 1–15. ISSN: 19961073. DOI: 10.3390/en11102659.

[54] Eli J. Wolf et al. “Designing Modules to Prevent Reverse Bias Degradation in Perovskite Solar Cells when Partial Shading Occurs”. In: *Solar RRL* 6.3 (Mar. 2022). ISSN: 2367198X. DOI: 10.1002/solr.202100239.

[55] Dongchen Lan and Martin A Green. “ll Perspective Combatting temperature and reverse-bias challenges facing perovskite solar cells”. In: *Joule* (2022), pp. 1–16. ISSN: 2542-4351. DOI: 10.1016/j.joule.2022.06.014. URL: https://doi.org/10.1016/j.joule.2022.06.014.

[56] Ming Hung Tseng et al. “Low-temperature gas-barrier films by atomic layer deposition for encapsulating organic light-emitting diodes”. In: *Nanotechnology* 27.29 (2016). ISSN: 13616528. DOI: 10.1088/0957-4484/27/29/295706.

[57] Tznng Fang Guo et al. “High performance polymer light-emitting diodes fabricated by a low temperature lamination process”. In: *Advanced Funtional Materials* 11.5 (2001), pp. 339–343. ISSN: 1616301X. DOI: 10.1002/1616-3028(200110)11:5<339::AID-ADFM339>3.0.CO;2-S.

[58] Bo Chen et al. “Imperfections and their passivation in halide perovskite solar cells”. In: *Chemical Society Reviews* 48.14 (2019), pp. 3842–3867. ISSN: 14604744. DOI: 10.1039/c8cs00853a.

[59] Mathworks. *Solar cell*. 2022. URL: https://nl.mathworks.com/help/physmod/sps/ref/solarcell.html (visited on 08/11/2022).

[60] G. Notton, V. Lazarov, and L. Stoyanov. “Optimal sizing of a grid-connected PV system for various PV module technologies and inclinations, inverter efficiency characteristics and locations”. In: *Renewable Energy* 35.2 (2010), pp. 541–554. ISSN: 09601481. DOI: 10.1016/j.renene.2009.07.013. URL: http://dx.doi.org/10.1016/j.renene.2009.07.013.

[61] Jayanta Deb Mondol, Yigzaw G. Yohanis, and Brian Norton. “Optimal sizing of array and inverter for grid-connected photovoltaic systems”. In: *Solar Energy* 80.12 (2006), pp. 1517–1539. ISSN: 0038092X. DOI: 10.1016/j.solener.2006.01.006.

# A

# Shading on the experimental setup

The actual shading performed on the experimental setup is shown in the figures below. An opaque black cardboard sheet was cut and placed at the holder positions to ensure the required module was completely shaded. Once the module and the cardboard cut-out are placed, it is locked in place. The light is illuminated directly above the holders, representing the AM1.5 spectrum.

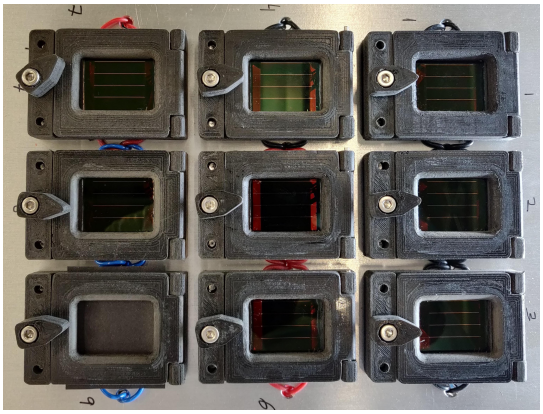

**Figure A.1:** Shading pattern 1

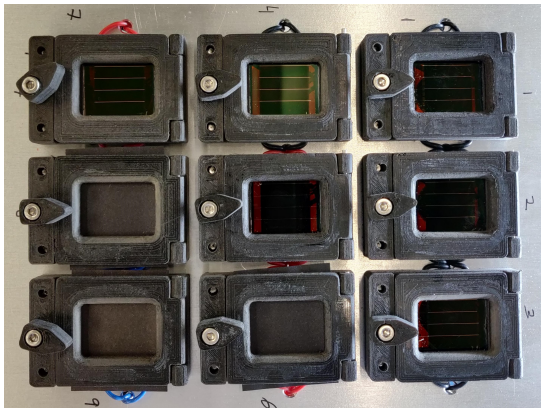

**Figure A.2:** Shading pattern 2

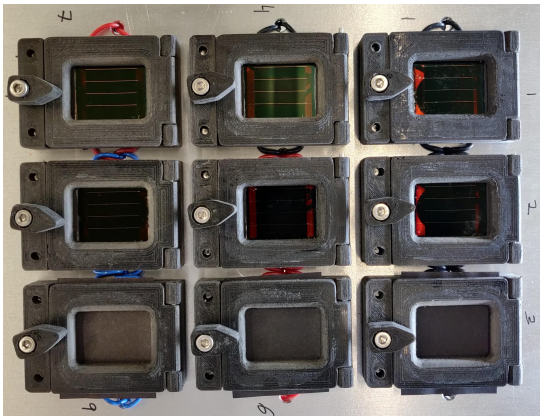

**Figure A.3:** Shading pattern 3

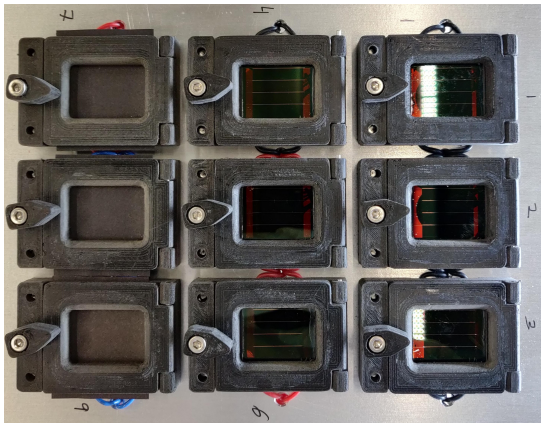

**Figure A.4:** Shading pattern 4

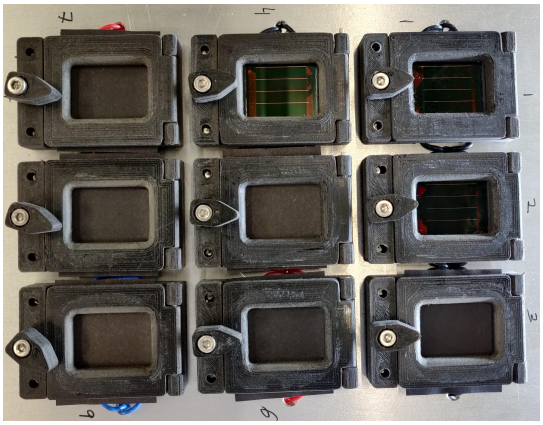

**Figure A.5:** Shading pattern 5

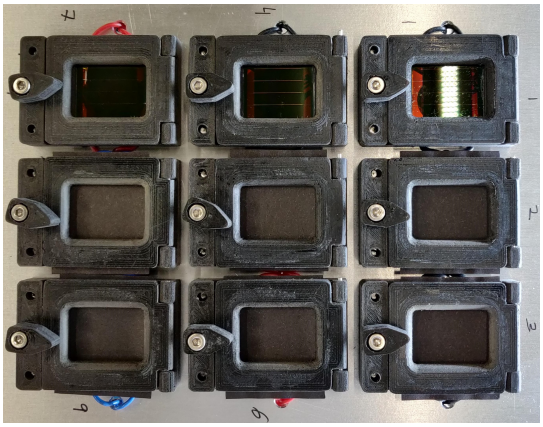

**Figure A.6:** Shading pattern 6

# B

# Simulink model

In this section, the Simulink model that was built to understand the response to shading of the different interconnections is illustrated. The model is shown in Figure B.1. The six different sub-blocks that are seen contain the model of each of the interconnections. The interface controls the irradiance for each of the solar modules in the interconnection in the image below. The irradiance can be changed by changing the constant block value. In the image, it is set to 1000 $W/m^2$, which can be changed to 0 for a full shade of a module. The nine constant blocks can be visualised as the module holders in Appendix A.

The modelling of the interconnection is showcased in Figure B.2 to Figure B.7. The model utilizes the solar cell blocks available in the Simulink block library to which the parameters obtained from IV fit software tool, shown in section 4.4 are appended [59]. The irradiance from the constant blocks is fed to the solar cell, and the resulting current and voltage for the respective interconnection is gathered in Matlab for plotting purposes.

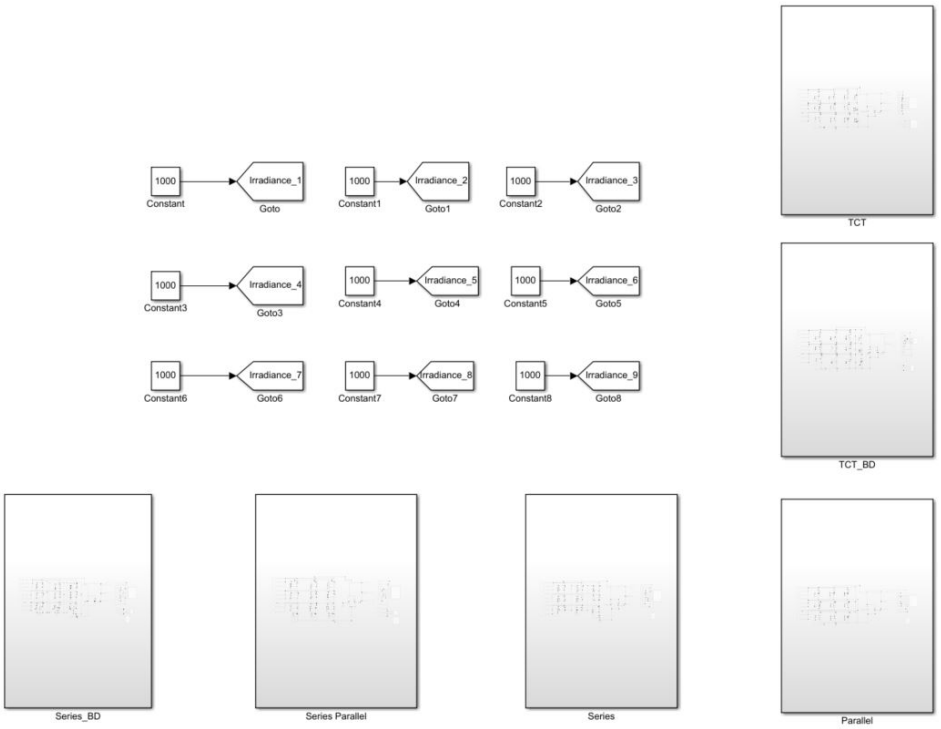


**Figure B.1:** Simulink model

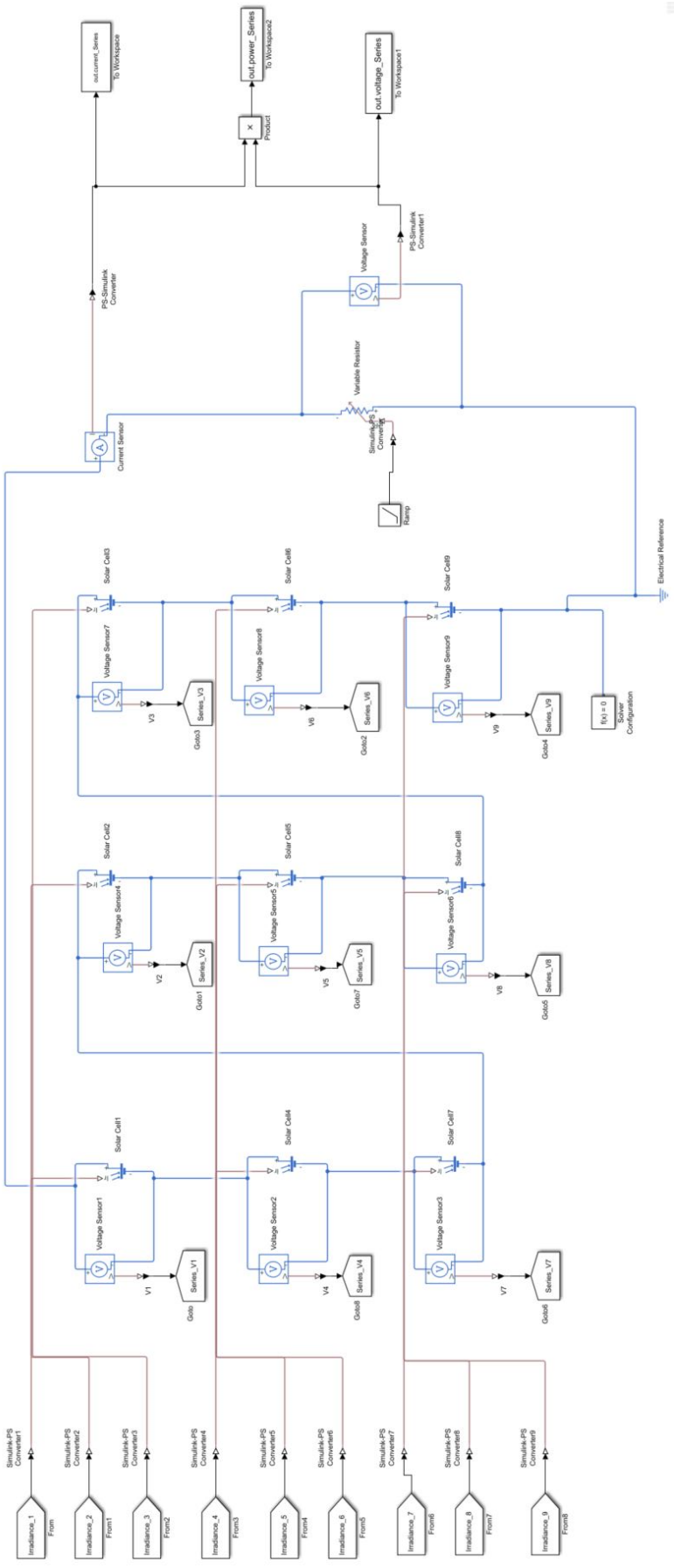


**Figure B.2:** Series interconnection

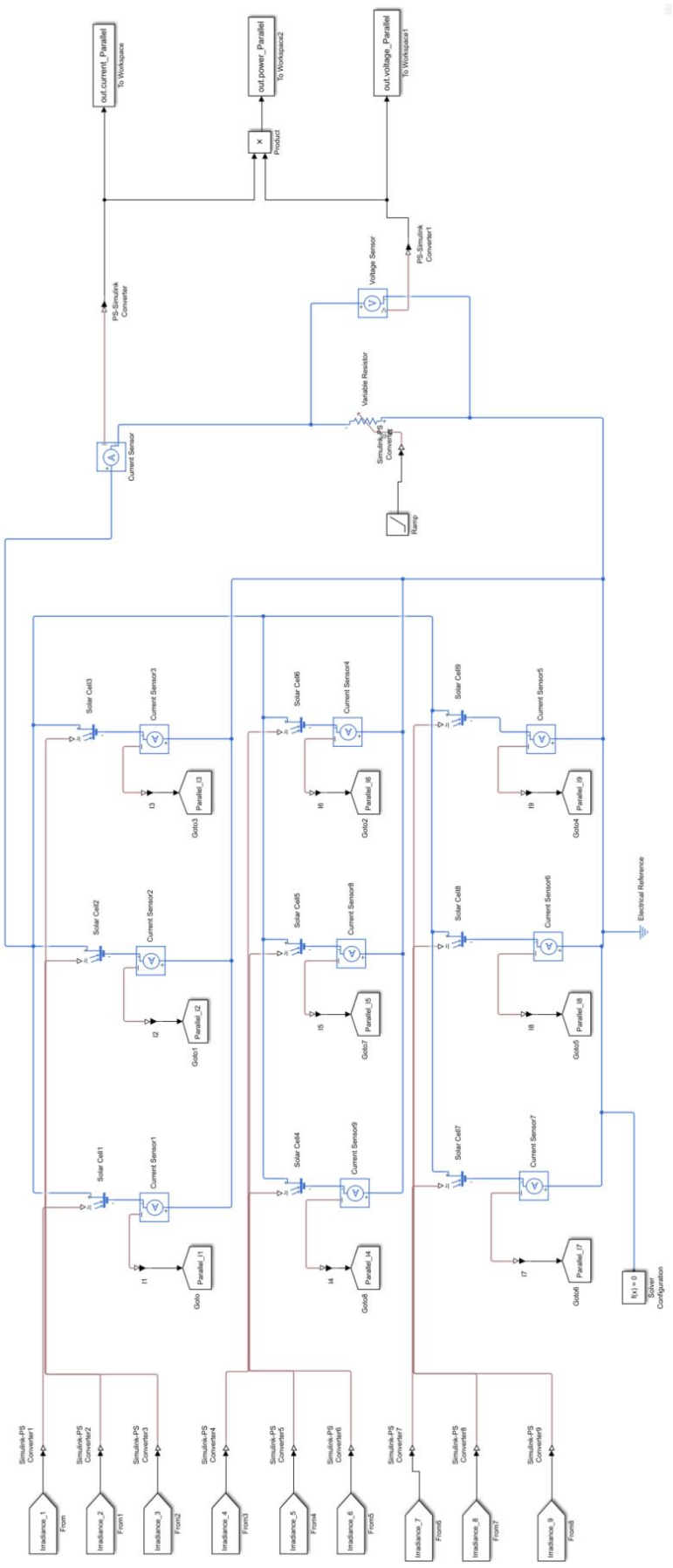


**Figure B.3:** Parallel interconnection

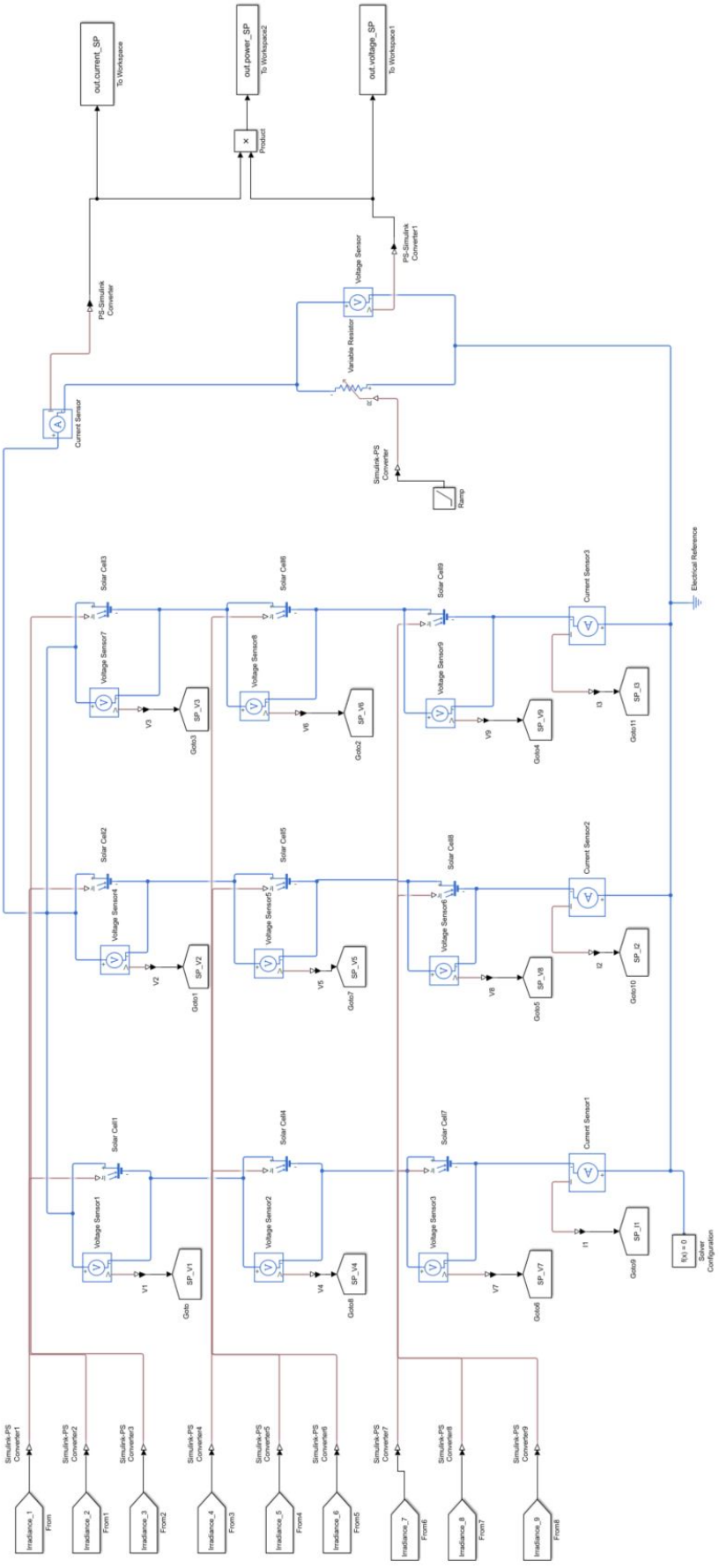


**Figure B.4:** Series-parallel interconnection

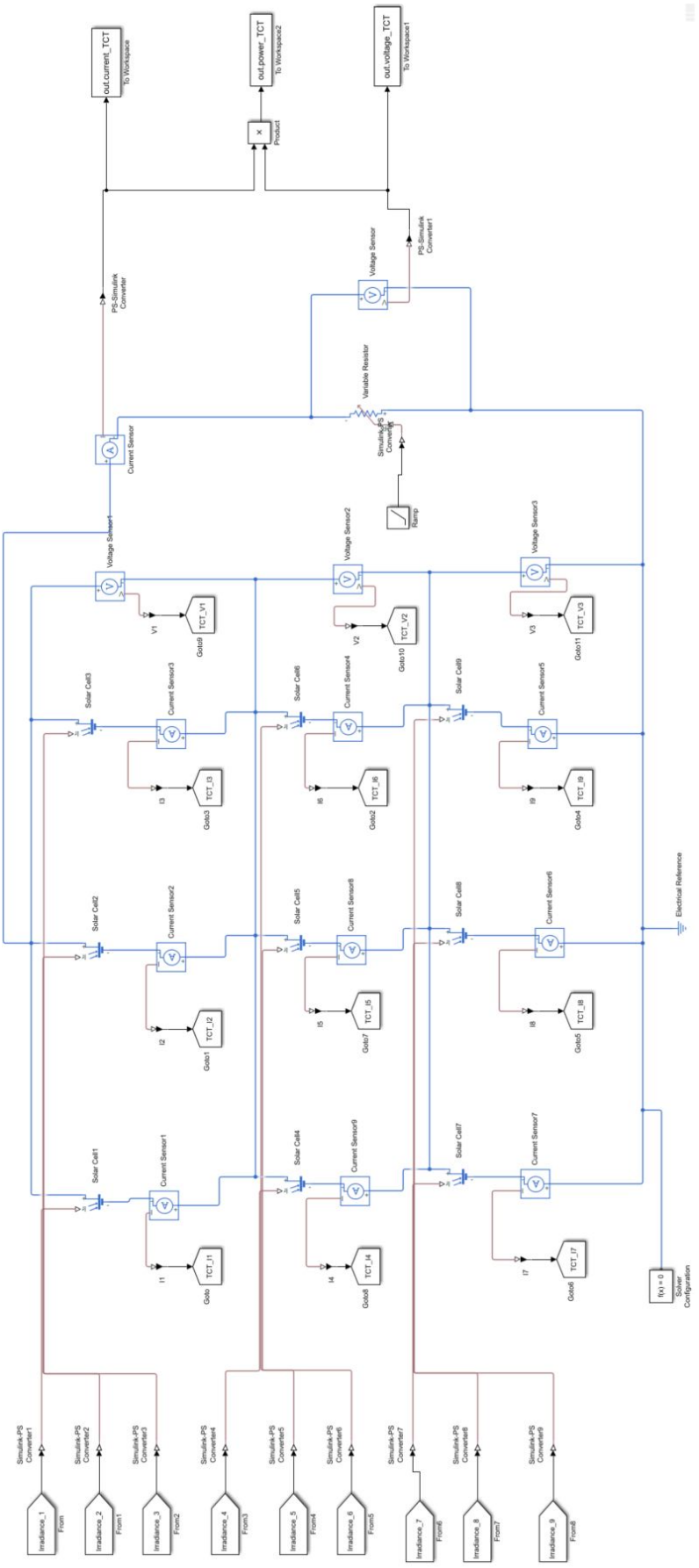


**Figure B.5:** TCT interconnection

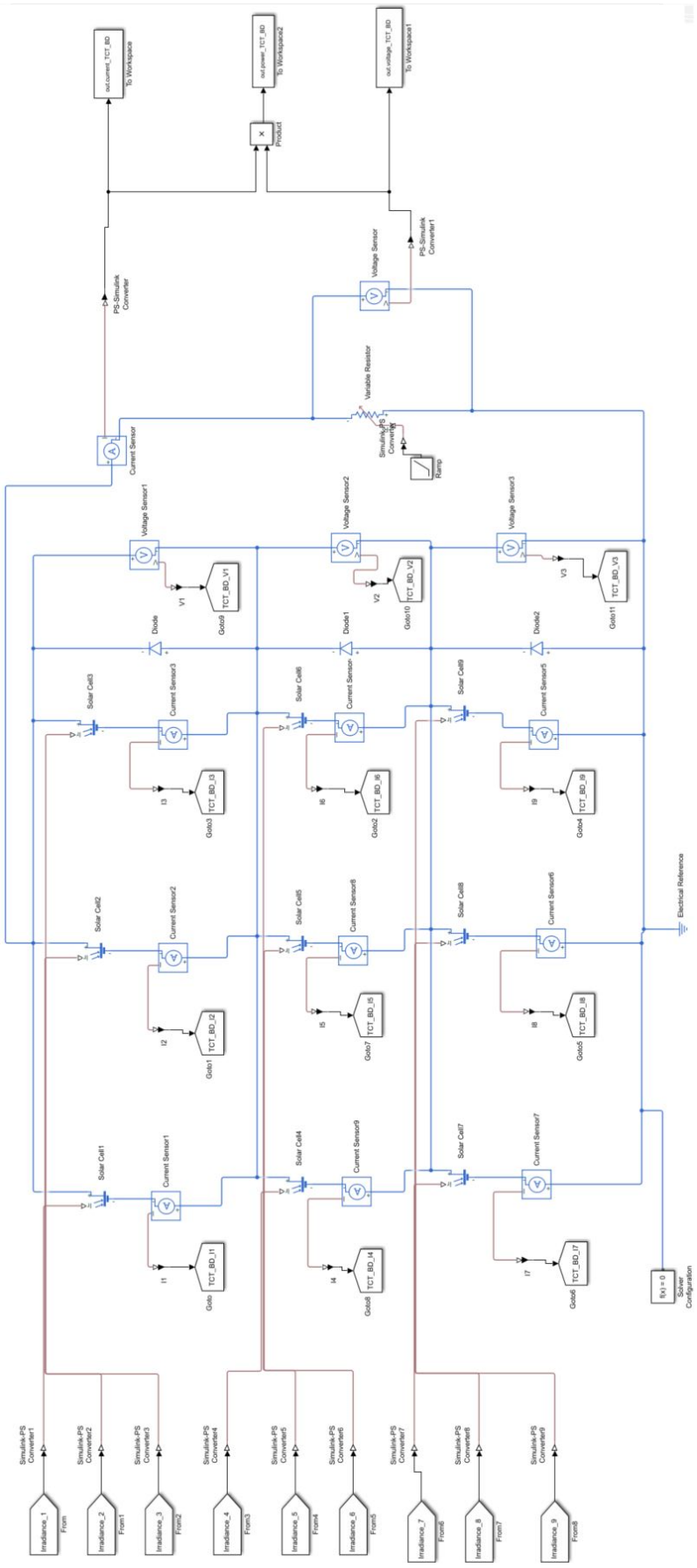


**Figure B.6:** TCT interconnection with bypass diodes

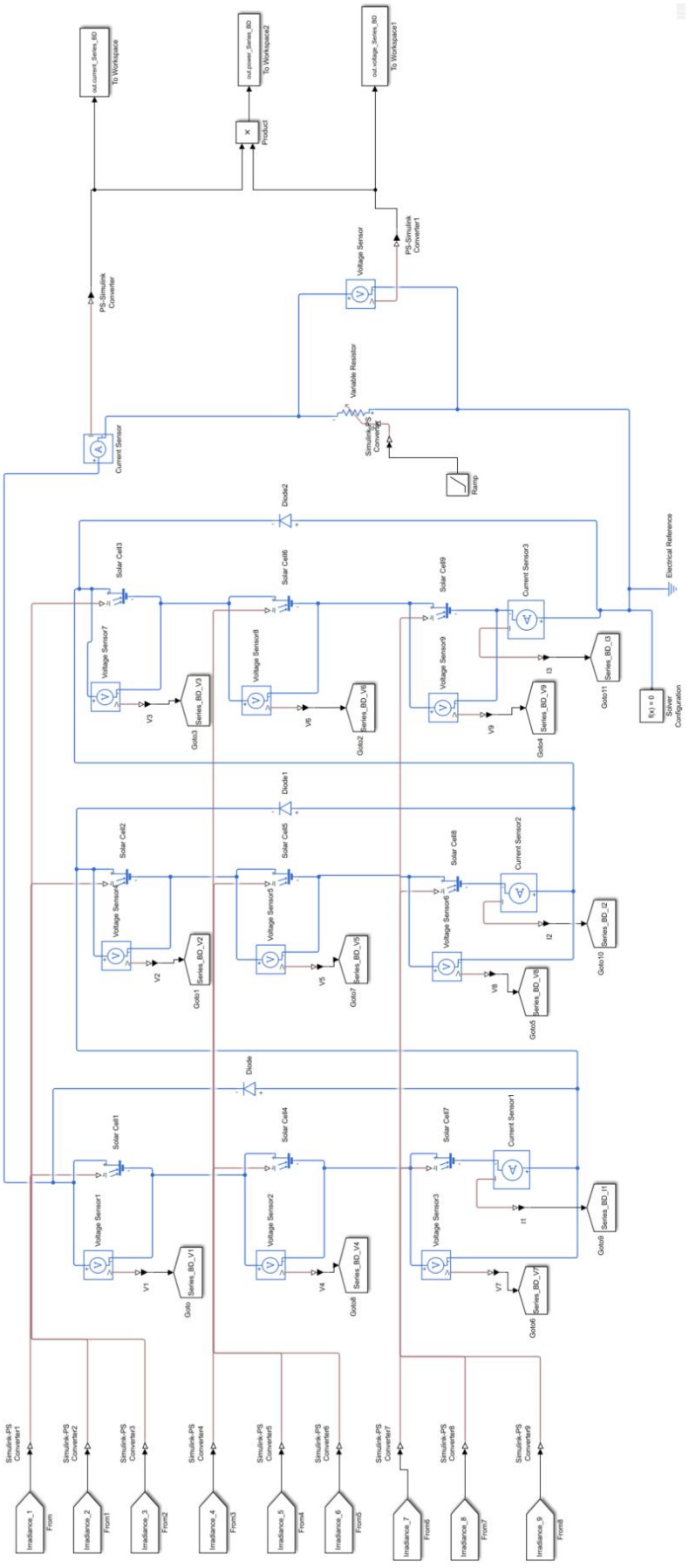


**Figure B.7:** Series interconnection with bypass diodes

# C

# Bypass diode

The connection of the bypass diodes to the TCT interconnection to perform the tests mentioned in section 5.4 is depicted in Figure C.1. The bypass diode is connected across the row of parallel modules. The diodes are held using crocodile clips in reverse bias orientation to the module.

The technical datasheet of the diode is included in the following pages. The diode's forward voltage is 1V, which means that the diode switches on when the reverse bias voltage across the module is greater than 1V.

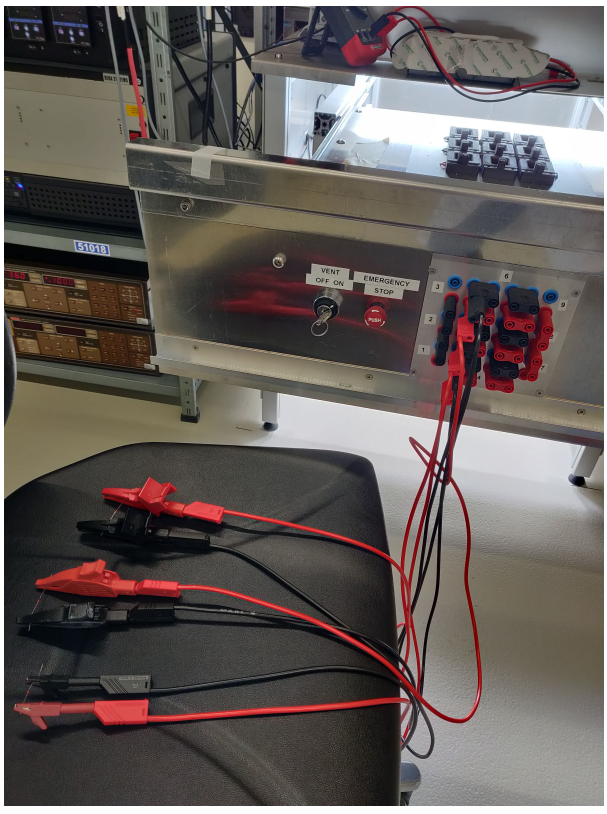


**Figure C.1:** Diode interconnection

# Small Signal Fast Switching Diodes

## FEATURES

- Silicon epitaxial planar diode
- Electrically equivalent diodes: 1N4148 - 1N914
- Material categorization: for definitions of compliance please see www.vishay.com/doc?99912

Pb e3 RoHS COMPLIANT HALOGEN FREE

## APPLICATIONS

- Extreme fast switches

**DESIGN SUPPORT TOOLS** click logo to get started

3D Models Available

## MECHANICAL DATA

**Case:** DO-35 (DO-204AH)

**Weight:** approx. 105 mg

**Cathode band color:** black

**Packaging codes / options:**

TR/10K per 13" reel (52 mm tape), 50K/box

TAP/10K per ammopack (52 mm tape), 50K/box

**PARTS TABLE**

| PART | ORDERING CODE | TYPE MARKING | CIRCUIT CONFIGURATION | REMARKS |
|---|---|---|---|---|
| 1N4148 | 1N4148-TAP or 1N4148TR | V4148 | Single | Tape and reel / ammopack |

**ABSOLUTE MAXIMUM RATINGS** ($T_{amb}$ = 25 °C, unless otherwise specified)

| PARAMETER | TEST CONDITION | SYMBOL | VALUE | UNIT |
|---|---|---|---|---|
| Repetitive peak reverse voltage | | $V_{RRM}$ | 100 | V |
| Reverse voltage | | $V_R$ | 75 | V |
| Peak forward surge current | $t_p$ = 1 µs | $I_{FSM}$ | 2 | A |
| Repetitive peak forward current | | $I_{FRM}$ | 500 | mA |
| Forward continuous current | | $I_F$ | 300 | mA |
| Average forward current | $V_R$ = 0 | $I_{F(AV)}$ | 150 | mA |
| Power dissipation | l = 4 mm, $T_L$ = 45 °C | $P_{tot}$ | 440 | mW |
| | l = 4 mm, $T_L \leq$ 25 °C | $P_{tot}$ | 500 | mW |

**THERMAL CHARACTERISTICS** ($T_{amb}$ = 25 °C, unless otherwise specified)

| PARAMETER | TEST CONDITION | SYMBOL | VALUE | UNIT |
|---|---|---|---|---|
| Thermal resistance junction to ambient air | l = 4 mm, $T_L$ = constant | $R_{thJA}$ | 350 | K/W |
| Junction temperature | | $T_j$ | 175 | °C |
| Storage temperature range | | $T_{stg}$ | -65 to +150 | °C |

| **ELECTRICAL CHARACTERISTICS** ($T_{amb}$ = 25 °C, unless otherwise specified) | | | | | | |
|---|---|---|---|---|---|---|
| **PARAMETER** | **TEST CONDITION** | **SYMBOL** | **MIN.** | **TYP.** | **MAX.** | **UNIT** |
| Forward voltage | $I_F$ = 10 mA | $V_F$ | | | 1 | V |
| Reverse current | $V_R$ = 20 V | $I_R$ | | | 25 | nA |
| | $V_R$ = 20 V, $T_j$ = 150 °C | $I_R$ | | | 50 | µA |
| | $V_R$ = 75 V | $I_R$ | | | 5 | µA |
| Breakdown voltage | $I_R$ = 100 µA, $t_p/T$ = 0.01, $t_p$ = 0.3 ms | $V_{(BR)}$ | 100 | | | V |
| Diode capacitance | $V_R$ = 0 V, f = 1 MHz, $V_{HF}$ = 50 mV | $C_D$ | | | 4 | pF |
| Rectification efficiency | $V_{HF}$ = 2 V, f = 100 MHz | $\eta_r$ | 45 | | | % |
| Reverse recovery time | $I_F$ = $I_R$ = 10 mA, $i_R$ = 1 mA | $t_{rr}$ | | | 8 | ns |
| | $I_F$ = 10 mA, $V_R$ = 6 V, $i_R$ = 0.1 x $I_R$, $R_L$ = 100 Ω | $t_{rr}$ | | | 4 | ns |

## TYPICAL CHARACTERISTICS ($T_{amb}$ = 25 °C, unless otherwise specified)

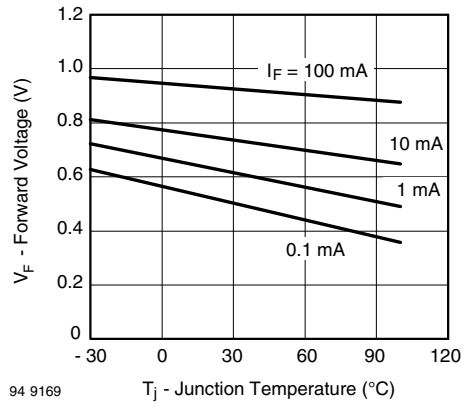


Fig. 1 - Forward Voltage vs. Junction Temperature

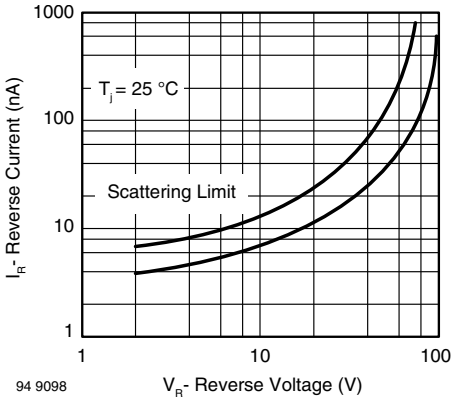


Fig. 3 - Reverse Current vs. Reverse Voltage

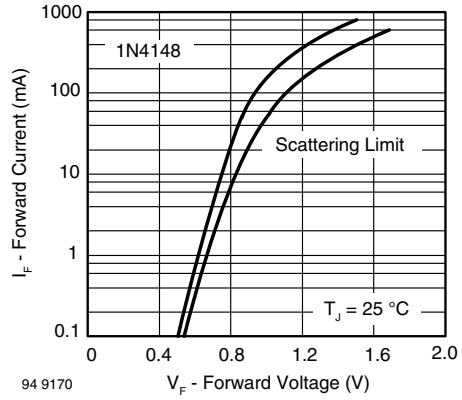


Fig. 2 - Forward Current vs. Forward Voltage

**PACKAGE DIMENSIONS** in millimeters (inches): **DO-35 (DO-204AH)**

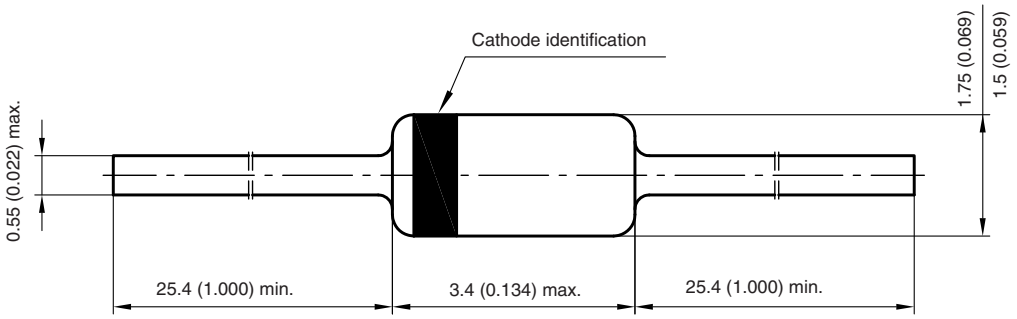


Document no.: 6.560-5004.12-4
Created - Date: 17. March 2008
21145

# D

# Voltage at different conditions

The voltage of each of the modules in the different interconnections was monitored in the model. Figure D.1 shows the voltage of the worst performing module in the interconnection when exposed to the shading patterns. The highest negative voltage shown in the figure is -18.27V, but this is impossible with a PSC as it breaks down at much lower voltages. The model shows such high voltages because it considers the same breakdown voltage as silicon by default, and it was not possible to change the parameter in Simulink. However, it gives an idea of which interconnection and shading pattern combinations can lead to degradation. In the cases where the voltage exceeds -6V, it will lead to degradation of the respective perovskite module.

| Interconnections | Shading patterns | Voltage (V) | | |
|---|---|---|---|---|
| | | SC | MPP | OC |
| Series | SP-0 | 0.00 | 2.67 | 3.52 |
| | SP-1 | -18.27 | -10.50 | -0.33 |
| | SP-2 | -6.80 | -3.41 | -0.25 |
| | SP-3 | -6.80 | -3.41 | -0.25 |
| | SP-4 | -6.80 | -3.41 | -0.25 |
| | SP-5 | -1.80 | -0.90 | -0.12 |
| | SP-6 | -1.80 | -0.90 | -0.12 |
| Parallel | SP-0 | 0.00 | 2.68 | 3.65 |
| | SP-1 | 0.00 | 2.67 | 3.60 |
| | SP-2 | 0.00 | 2.58 | 3.49 |
| | SP-3 | 0.00 | 2.58 | 3.49 |
| | SP-4 | 0.00 | 2.58 | 3.49 |
| | SP-5 | 0.00 | 2.29 | 3.16 |
| | SP-6 | 0.00 | 2.29 | 3.16 |
| Series Parallel | SP-0 | 0.00 | 2.68 | 3.64 |
| | SP-1 | -6.80 | 0.42 | 3.07 |
| | SP-2 | -6.80 | -0.33 | 2.51 |
| | SP-3 | -6.80 | -3.41 | -0.03 |
| | SP-4 | 0.00 | 2.58 | 3.49 |
| | SP-5 | -6.80 | -4.54 | -2.29 |
| | SP-6 | -1.80 | -0.90 | -0.01 |
| TCT | SP-0 | 0.00 | 2.68 | 3.64 |
| | SP-1 | -4.40 | 2.08 | 3.48 |
| | SP-2 | -5.02 | 0.63 | 3.16 |
| | SP-3 | -6.80 | -3.41 | -0.03 |
| | SP-4 | 0.00 | 2.58 | 3.49 |
| | SP-5 | -5.08 | -2.75 | -0.03 |
| | SP-6 | -1.80 | -0.90 | -0.01 |
| TCT-BD | SP-0 | 0.00 | 2.68 | 3.64 |
| | SP-1 | -0.60 | 2.08 | 3.48 |
| | SP-2 | -0.61 | 0.63 | 3.16 |
| | SP-3 | -0.62 | -0.60 | -0.03 |
| | SP-4 | 0.00 | 2.58 | 3.49 |
| | SP-5 | -0.61 | -0.60 | -0.03 |
| | SP-6 | -0.61 | -0.60 | -0.01 |
| Series-BD | SP-0 | 0.00 | 2.68 | 3.52 |
| | SP-1 | -7.36 | -7.36 | -0.34 |
| | SP-2 | -7.36 | -7.36 | -0.25 |
| | SP-3 | -6.80 | -3.41 | -0.25 |
| | SP-4 | -0.20 | -0.20 | -0.20 |
| | SP-5 | -5.69 | -2.85 | -0.12 |
| | SP-6 | -1.80 | -0.90 | -0.12 |

**Figure D.1:** Current and voltage at SC, MPP and OC conditions

# E

# Degradation of the modules during lamination

Figure E.1 shows IV curve of all modules used in the shading test for TCT interconnection with bypass diodes. However, after the lamination of the module at 130°C, the modules are degraded with an average drop in efficiency of about 4%, from 16% to 12% as depicted in Figure E.2. The degradation is not identical in all modules, with some undergoing worse degradation than few other ones. The reason for the difference in performance can be due to small differences in the lamination process as it was performed by hand. There is a wavy pattern that emerges in the plot after lamination, this is suspected to be due to the uneven interface between the encapsulant and the deposition layers of the module obstructing the flow of current.

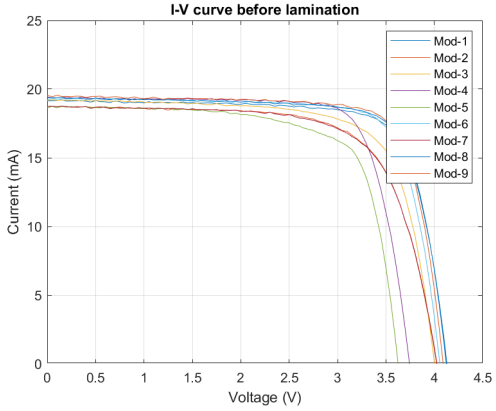


**Figure E.1:** IV curve of modules before lamination

Interestingly, the wavy pattern in the plot disappears after 5 days in the glove box as shown in Figure E.3. The reason can be due to a curing process that happens in the glove box leading to a more even interface between the encapsulant and deposition layers. Again, it appears to affect not all modules equally, as some have an increased $V_{oc}$. Possible cause for the increase in $V_{oc}$ could be due to the formation of cracks within the cells, leading to the creation of sub-cells within the module. The lamination process appears to affect the structural integrity of the PSC module. Higher lamination temperature need to avoided if possible and other techniques of lamination need to be explored.

For the tests described in section 5.4, it was conducted immediately after lamination. Therefore, the IV plot shown in Figure E.2 is considered to represent the module characterictics.

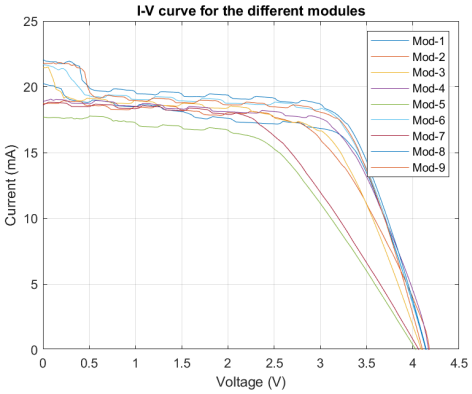


**Figure E.2:** IV curve of modules immediately after lamination

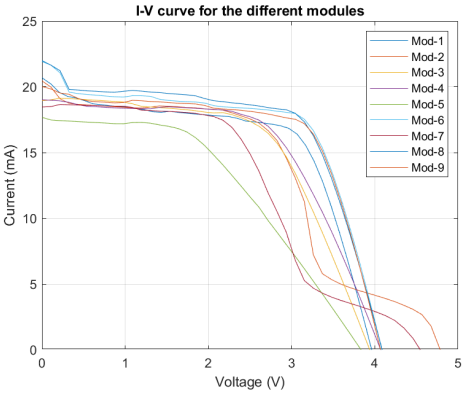


**Figure E.3:** IV curve after 5 days of lamination

# F

# Inverter losses

The inverter's efficiency is a function of input voltage and power, among other factors. Ideally, the input power to the inverter needs to be closely matched to the inverter's rated power, and the input voltage must be in the range of rated voltage. Deviations in either parameter leads to significant losses as depicted in Figure F.1. Typically, the cells are stringed together in series in a solar panel to increase the voltage. Such panels may then be connected in series to match the rated input voltage of the inverter. Conversely, if the cells are to be connected in parallel, it leads to no voltage build-up. It leads to a high difference in the input and the rated voltages of the inverter, contributing to high losses in the systems apart from the significant resistive losses due to high current [60] [61].

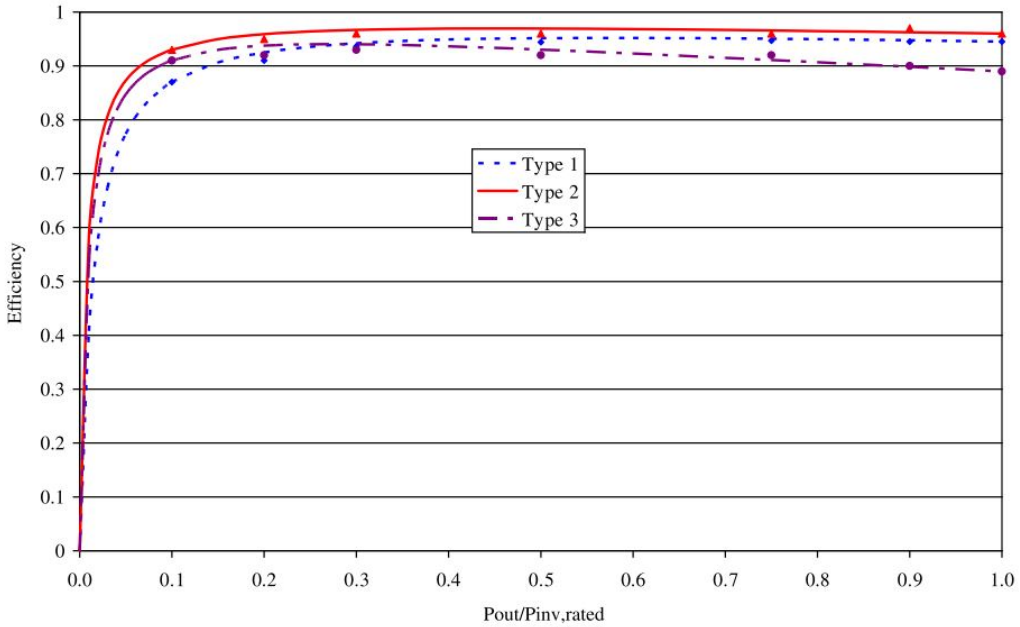


**Figure F.1:** Inverter efficiency plotted against power ratio [60]